To the Graduate Council:

I am submitting herewith a thesis written by Rodney William Hoefer entitled "A Study of Turbulent Flow in a Superheater Model Using Laser Velocimetry." I have examined the final copy of this thesis for form and content and recommend that it be accepted in partial fulfillment of the requirements for the degree of Master of Science, with a major in Mechanical Engineering.

Roy J. Schulz

Roy J. Schulz, Major Professor

We have read this thesis and recommend its acceptance:

[illegible] Crawford

Thomas V. Gill [illegible]

Accepted for the Council:

[illegible] Minkel

Vice Provost
and Dean of The Graduate School

STATEMENT OF PERMISSION TO USE

In presenting this thesis in partial fulfillment of the requirements for a Master's degree at The University of Tennessee, Knoxville, I agree that the Library shall make it available to borrowers under rules of the Library. Brief quotations from this thesis are allowable without special permission, provided that accurate acknowledgment of source is made.

Permission of extensive quotation from or reproduction of this thesis may be granted by my major professor, or in his absence, by the Head of Interlibrary Services when, in the opinion of either, the proposed use of the material is for scholarly purposes. Any copying or use of the material in this thesis for financial gain shall not be allowed without my written permission.

Signature Rodney W. Hoefer

Date November 1985

A STUDY OF TURBULENT FLOW IN A SUPERHEATER MODEL USING LASER VELOCIMETRY

A Thesis

Presented for the

Master of Science

Degree

The University of Tennessee, Knoxville

Rodney W. Hoefer

December 1985

DEDICATION

This thesis is dedicated to my wife, Mrs. Dianna Lynn Hoefer.

ACKNOWLEDGMENTS

The work reported herein was supported by The University of Tennessee Space Institute Energy Conversion Research and Development Programs under Contract No. DE-AC02-79ET10815.

The author would like to express his appreciation to the members of his committee, Dr. Roy J. Schulz, Chairman, Dr. Thomas V. Giel, Jr., and Dr. Lloyd W. Crawford. Appreciation is also expressed to Dr. Giel for his assistance with the laser velocimeter system used in the study. The author would also like to thank Mr. William P. Millard and Mr. Bradley Winkleman for their assistance in setting up the experiment. Special appreciation is expressed to Ms. Madge Gibson for typing the thesis.

The author would also like to thank Mr. John P. Foote who provided invaluable assistance throughout the investigation.

ABSTRACT

An experimental study was conducted of the turbulent flow in a model superheater using laser velocimetry. The primary objective of the superheater model study was to determine the aerodynamic behavior of the gas flow through the superheater in order to help explain heat transfer and ash deposition characteristics of the superheater.

The 1/4 scale superheater model used air at standard conditions to generate sufficiently high Reynolds number flows in the model. Two component vector velocity data was obtained using a dual Bragg cell laser velocimeter. Measurements of mean velocity, turbulence intensity, and velocity-time data were obtained at many axial stations along the flow.

The data from the superheater model study showed that nonuniform flow conditions exist in the first section of the superheater. This flow nonuniformity is expected to reduce the efficiency of the superheater operation because of the effects on heat transfer and ash deposition. The flow becomes uniform after the gas has passed through enough tube banks. Periodic flow oscillations occur behind each row of cooling tubes because of vortex shedding. Wakes occurring behind each row of tubes increase turbulence intensity which is expected to increase ash deposition in real superheaters. No large scale flow unsteadiness was found in frequency analysis of the data.

TABLE OF CONTENTS

LIST OF FIGURES

FIGURE PAGE

1.0 INTRODUCTION

1.1 The Coal Fired Flow Facility at UTSI

Electrical utilities typically operate at efficiencies of about 33 to 36 percent. In order to develop utilities with higher efficiencies, a magnetohydrodynamic (MHD) topping cycle is being studied at The University of Tennessee Space Institute (UTSI) in the United States Department of Energy's Coal Fired Flow Facility (CFFF). MHD power generation [1] occurs when an electrically conductive fluid flows through a magnetic field to convert part of the energy of the fluid into electrical energy. The CFFF open cycle coal-fired MHD flow train is designed for a thermal input of 28 MW.

At the CFFF, which is shown in Figure 1, page 40, the primary combustor [2] mixes and burns the preheated oxidizer from the vitiation heater with pulverized coal, seed (potassium carbonate), and fuel oil achieving temperatures at about 3000K and conductivities approaching 10 $\frac{\text{mhos}}{\text{m}}$. The combustor operates fuel rich to minimize NO_x formation. The conductive gas or plasma then passes through a converging-diverging nozzle to accelerate the combustion plasma to a Mach number near 1.2 through the generator to the diffuser. The diffuser recovers static pressure and reduces the flow velocity to a level acceptable for the downstream steam plant components. From the diffuser, the gas passes through the radiant slagging furnace where most of the slag is removed, the gas is used to boil water, and controlled gas cooling occurs to control nitrogen oxide decomposition. The potassium from the seed which has combined with the sulfur in the coal, begins to condense near the furnace exit. Next, the gas and potassium sulfate pass through the secondary combustor to be mixed with air and to burn the remaining combustibles. From the secondary combustor, the gas travels through a special superheater designed to test materials, ash deposition, corrosion and also superheat steam as in a typical steam power plant. The gas exits the superheater into an air heater to preheat air for the secondary combustor. Finally, particulates are removed from the gas by a baghouse, electrostatic precipitator, or a wet venturi scrubber before the gas is exhausted into the atmosphere.

1.2 The CFFF Superheater

The superheater test module (SHTM) [3] at the CFFF experiences the flue gas environment and tube temperatures expected in MHD superheaters to permit evaluation of fouling, corrosion, and heat transfer in such devices. Because of the different MHD gas composition, particularly the high K_2SO_4 content, the fouling, corrosion, and heat transfer characterics are expected to differ considerably from the standard coal-fired utility superheater. The SHTM contains both steam-cooled tubes and water-cooled tubes in a horizontal, rectangular duct. The SHTM is divided into steam-cooled test sections and water-cooled cooling sections. The duct is nominally 1.22 m (4 ft) wide and 2.29 m (7.5 ft) high. Table 1 lists the design temperatures for the SHTM. The SHTM receives combustion gas from the ash-seed hopper of the secondary combustor at a design temperature of nominally 1260°C (2300°F) and delivers it to the air heater at about 427°C (800°F).

Table 1. Design Temperatures for the SHTM.

Location	Temperature
Entrance	2300°F
Test Section 1	2300°F
Cooling Section	1550°F
Test Section 2	1110°F
Exit	800°F
Temperature of water in cooling tubes	70°F
Temperature of steam in steam tubes	387°F

Steam-cooled tube banks were designed to provide a way to test fouling and corrosion characteristics. Sootblowers are currently used to control the accumulation of potassium sulfate and ash on these tubes. Water-cooled tube banks are used between the superheater test sections to accelerate the gas cooling between test sections and before the gas enters the air heater. Temperatures of the gas and the tubes throughout the SHTM are dependent on the equilibrium thickness and extent of tube fouling, which is presently unknown and is to be determined by experiment. The SHTM, which is shown in Figure 2, page 41, consists of an inlet transition, three steam-cooled test sections, five water-cooled sections, and a 180° elbow. The inlet transition increases the gas flow area from 2.01 m^2 (21.66 ft^2) at the ash-seed hopper exit to 2.82 m^2 (30.43 ft^2) at the entrance of Test Section 1 (TS1) which is shown in Figure 3, page 42. TS1 contains a 4-pass water-cooled tube bundle or screen followed by a 2-pass steam-cooled test bank. The water-cooled screen has eight 63.5 mm (2.5 in.) O.D. approximately 2.29 m (7.5 ft) long pendant tubes per row with a 0.153 m (6 in) side spacing. The rows are in line on 0.254 m (10 in) centers. In addition to cooling the flue gas, these tubes serve as a radiation screen and as an ash-seed screen. Tubes were selected that were large enough to maximize cooling while minimizing the flow blockage. The steam-cooled test bank consists of eight 38.1 mm (1.5 in) O.D. tubes on 0.153 m (6 in) transverse centers and two in-line rows on 0.153 m (6 in) centers. Following TS1 are two cooling sections. Each cooling section, shown in Figure 4, page 43, consists of 12 in-line passes of eight 63.5 mm (2.5 in) O.D. water-cooled tubes on 0.153 m (6 in) transverse centers, and 0.254 m (10 in) longtitudinal centers. Next is Test Section 2 (TS2), shown in Figure 5, page 44, which consists of two in-line passes of eight 38.1 mm (1.5 in) O.D. pendant tubes on 0.153 m (6 in) transverse centers and 0.153 m (6 in) longtitudinal centers. Following TS2 are, respectively, Cooling Section 3, Test Section 3, Cooling Section 4, a 180° elbow, and Cooling Section 5. After leaving Cooling Section 5, the gas flows through a transition section into the air heater.

1.3 Purpose of the Superheater Model Study

To understand and possibly improve the operation of the superheater and the design of future MHD systems, the following information is needed:

1. The aerodynamic behavior of the gas flow such as the mean velocity fields and turbulence characteristics.
2. Identification of any periodic or random flow oscillations caused by vortex formation and shedding.
3. Identification of any nonuniform inlet velocity profiles caused by the geometric configuration of the ash-seed hopper and the inlet transition.
4. Determination if the flow profiles become uniform, and if so, at what axial station this occurs.
5. The effects of different top and bottom wall geometries such as the ash-seed hopper cavities in the superheater.

In turn, this information will help explain:

1. Heat transfer through the steam tubes and the superheater walls.

2. Application of refractory to the inner walls of the superheater.
3. Ash deposition characteristics.
4. The effect of ash deposition on heat transfer in the superheater.
5. The effectiveness of devices used to reduce ash deposition such as sootblowers.
6. Erosion of the tubes.

The flow characteristics of the superheater are more easily acquired, and can be acquired in greater detail, in a clear walled, subscale, isothermal flow model. Therefore, such a model was built for this study.

2.0 EXPERIMENT DESIGN

2.1 Design and Construction of the Superheater Model

A one-fourth scale air flow model was constructed with the same configuration as the CFFF superheater. The superheater model and the measurement coordinate system are illustrated in Figure 6, page 45. The sections of the CFFF Low Mass Flow train that were modeled include the ash-seed hopper, the inlet transition, Test Section 1, one cooling section, and Test Section 2. The ash-seed hopper section was constructed to create the same flow entering the superheater section of the model as in the CFFF superheater. A honeycomb flow straightener was installed at the inlet of the ash-seed hopper section to eliminate the effects on the flow caused by the flexible ducting which carried the air from outside the test building into the model. Air at standard conditions was pulled through the model by a backwardly inclined, adjustable speed centrifugal fan. Flexible ducting was used to carry the air from the model outlet transition to the fan and also to carry air from the fan to the outside wall of the test building where the air is exhausted into the atmosphere. The air flow rate was measured with a pitot tube and manometer which were located at the entrance of the ash-seed hopper section. The ash-seed hopper section and the outlet transition were fabricated from 3.2 mm (1/8 in) aluminum plate. The inlet transition, Test Section 1, the cooling section, and Test Section 2 were fabricated from 3.2 mm (1.8 in) acrylic plate to allow measurements to be taken with a laser velocimeter. The superheater model and the laser velocimeter set-up are shown in Figure 7, page 46. The cooling tubes were constructed with 15.9 mm (5/8 in) O.D. acrylic tubing, 15.4 mm (5.8 in) O.D. copper tubing, and 15.9 mm (5/8 in) O.D. copper elbows with a 90° bend. The steam tubes were constructed with 9.5 mm (3/8 in) O.D. acrylic tubing, 9.5 mm (3/8 in) O.D. copper tubing, and 9.5 mm (3/8 in) O.D. copper elbows with a 90° bend. The tubes were supported inside the model with number 6 threaded rod. The superheater model was mounted on a stand on its side so that the top wall of the superheater was facing the LV system. The model was mounted this way so that velocity measurements could be taken completely around the tubes and because of limited vertical traverse of a modified milling machine bed on which the LV system was mounted. A water spray nozzle was used to provide seeding for the laser velocimeter and was mounted inside a 0.30 m (12 in) O.D. PVC duct outside the test building. A fine water particle mist was sprayed through the PVC duct into the superheater model system entrance, which prevented wind from affecting the seeding rate.

2.2 Test Conditions

Aerodynamic flow conditions in the model need to be identical to those in the superheater at the CFFF. This can best be accomplished by acquiring the same Reynolds number in the model as in the CFFF superheater. The Reynolds number is given by [4]:

$$Re = \frac{V\rho \; D_{CH}}{\mu} \qquad (1)$$

where V is the velocity of the gas, ρ is the density of the gas, and μ is the viscosity. D_{CH} is the equivalent diameter for a rectangular duct and is given by:

$$D_{CH} = \frac{2ab}{(a + b)} \tag{2}$$

where a is the height and b is the width of the rectangular duct. For the CFFF superheater, a is 2.29 m (7.5 ft) and b is 1.22 m (4 ft), giving D_{CH} = 1.59 m. The average temperature and pressure from the inlet transition to test section no. 2 of the superheater are 900°C (1650°F) and 9.65×10^4 N/m^2 (14 lbf/in^2). The mass flow rate is 5.90 Kg/s (13 lbm/s). At these conditions the velocity of the gas is 6.46 m/s (21.18 ft/s), the density is 0.30 kg/m^3 (0.0187 lbm/ft^3), and the viscosity coefficient is 4.60×10^{-5} Kg/m-s (0.1112 lbm/ft-hr). The Reynolds number is then calculated to be Re = 6.70×10^4. At this Reynolds number a duct flow is turbulent. From the Reynolds number of the CFFF superheater, the scaled velocity and volume flow rate can be determined for the superheater model. The velocity can be found by rearranging equation (1) to obtain:

$$V = \frac{Re\ \mu}{D_{CH}\ \rho}\ . \tag{3}$$

Air at standard conditions is the working medium used in the model and has the following properties: the density is 1.21 kg/m^3 (0.0756 lbm/ft^3), and the viscosity coefficient is 2.23×10^{-5} Kg/m-s (1.50×10^{-5} lbm/ft-s). The equivalent diameter, D_{CH}, for the 1/4 scale model is 0.41 m (1.33 ft). Knowing these properties, the needed velocity at the model entrance was determined to be V = 3.04 m/s. The volume flow rate, Q, was then calculated by:

$$Q = VA \tag{4}$$

where V is the velocity of the air and A is the cross-sectional area of the duct. For the superheater model, the cross-sectional area is 0.19 m^2 (2.00 ft^2). Therefore, the volume flow rate for the model was Q = 0.58 m^3/s or 1224 CFM.

Another Reynolds number was calculated for tube heat transfer using the film properties for a hot gas and a cooled tube wall. This Reynolds number is given by:

$$Re = \frac{\rho_f V_g D_T}{\mu_f} \tag{5}$$

where ρ_f is the film density, V_g is the velocity of the gas between the tubes, D_T is the diameter of the tube, and μ_f is the film viscosity coefficient. At Test Section 1, the gas temperature is 1174°C (2170°F), the fluid temperature is 157°C (340°F), and the film temperature is 665°C (1255°F). At these temperatures, $\rho_f = 0.352$ Kg/m^3 (0.022 lbm/ft^3), D_T = 63.5 mm (2.5 in), and $\mu_f = 4.05 \times 10^{-5}$ Kg/m-s (2.72×10^{-5} lbm/ft-s) which gives $Re = 9.9 \times 10^3$. This Reynolds number for the full-scale SHTM is much smaller than the value based on D_{CH}. The primary purpose of the superheater model study was to determine bulk flow characteristics, and so the first Reynolds number was used for the model design.

2.3 Laser Velocimeter Measurement Technique

A laser velocimeter (LV) was chosen to make velocity measurements in the superheater model because an LV does not interact with the flow and can provide very accurate measurements in turbulent flow even when the flow reverses direction, provided that appropriate seeding of the flow can be achieved. The LV measures velocity by detecting the Doppler frequency shift of scattered light from a particle moving in the flow.

In an LV system, the laser provides a coherent light beam which is diffracted into 2 or more beams which are then refocused to form a probe volume. These beams have the same wavelength, λ, and intersect at an angle, θ. When the probe volume is formed by the intersecting beams, fringes are produced. The fringe spacing, δ, is given by [5]:

$$\delta = \frac{\lambda}{2 \sin \theta/2}. \tag{6}$$

As a particle moves across the fringe pattern, it scatters light with a frequency, f, that is directly proportional to the velocity component, u, which is normal to the fringes. This velocity component is determined by:

$$u = \delta \times f. \tag{7}$$

When the velocity direction is unknown, which is the case for the superheater model study, it is necessary to use a Bragg cell. A Bragg cell generates moving ultrasonic waves with constant frequency using a vibrating crystal. As the laser beam passes through the Bragg cell, it is diffracted into several frequency shifted beams. In the two component Bragg cell used at UTSI, two orthogonally mounted crystals diffract the entering beam in two directions. The four central beams are of near equal intensity and are frequency shifted in increments of the crystal frequencies. An optical system directs these four beams to converge at the probe volume where both a set of horizontal fringes and a set of vertical fringes are produced, thus allowing measurements to be made for two components of velocity. These fringes move across the probe volume at the different respective crystal frequencies. Thus a stationary particle scatters light from the fringes at two crystal frequencies, and a particle moving with or against the fringes scatters light at frequencies of u/δ below or above the crystal frequencies, respectively. Driving the crystals at different frequencies (i.e., 15 and 25 MHz) makes it possible to separate the velocity components using band-pass frequency filtering, if $u/\delta \ll 15$ or 25 MHz.

2.4 Laser Velocimeter Operation

The laser velocimeter system used in the superheater model study included a 3 watt argon ion laser, a beam collimator, a Bragg cell, two front surface mirrors, three transmitting lenses, two collector lenses, and two photomultiplier tubes. The LV system is illustrated in Figure 8, page 47. The laser velocimeter system was positioned on a modified milling machine bed that traverses in three dimensions. The modified milling machine bed was equipped with a digital position indicator that was used to position the laser velocimeter probe volume throughout the model. The milling machine bed wheels were positioned on rails so that it could easily be moved parallel to the front of the model so that velocity measurements could be taken along the complete length of the model. The argon ion laser produces a beam that was reflected 90° by a front surface mirror. The beam passed through the Bragg cell which diffracted the laser beam into four beams by frequency shifting the horizontal velocity component beam by approximately 15 MHz and the vertical velocity component beam by approximately 25 MHz. The beams were then reflected 180° by another front surface mirror into the beam expander lens pair. The first lens causes the four beams to converge at a point and then expand to a larger spacing before reaching the second lens. The second lens aligns the four beams so that they are parallel as they are directed to the third transmitting lens. The third lens causes the four beams to converge into the probe volume where velocity measurements are taken.

The collector lenses focus light scattered from the probe volume onto the photomultiplier tubes. Apertures are mounted in front of the photomultiplier tubes to minimize the probe volume length and filter out undesired background light. A microprocessor was used to control the signal processor electronics. The signal to the photomultiplier tube has a strong 15 MHz spectral band, two weak 10 and 40 MHz spectral bands, and a strong 25 MHz spectral band. This signal is divided into two equal parts by a signal splitter. The two parts are sent to radio frequency mixers which are driven by a phase-locked-loop (PLL) oscillator. The mixers have an intermediate frequency port in which a sum and a difference of the radio frequencies and the local oscillator frequencies are output. The low pass filter eliminates all but the difference frequency. Because of this process, signal frequencies can be measured more accurately and noise is reduced.

Burst counter signal processors measure the average period of each signal by counting the number of cycles of a 100 MHz clock over a fixed number of signal cycles. This fixed number of signal cycles is called the long clock count. A short clock count is taken simultaneously with the long clock count to check the periodicity of each measurement. An adjustable zero crossing detector is used to minimize noise pulses and logic circuits are used to eliminate faulty signals. Knowing the number of clock cycles counted, n, the timer rate, t, and the clock count, c, the signal frequency, f, can be calculated from:

$$f = \frac{c}{nt}. \tag{8}$$

A reference frequency, f_o, is found by taking the difference between the Bragg cell frequency, f_{BC}, and the local oscillator frequency, f_{LO}, or:

$$f_o = f_{BC} - f_{LO}. \tag{9}$$

Using the signal frequency, f, the reference frequency, f_o, and the fringe spacing, δ, the velocity can be found using the formula:

$$u = \delta(|f_o| - f) \text{ when } f_o > 0,$$
$$u = \delta(f - |f_o|) \text{ when } f_o < 0. \tag{10}$$

2.5 Data Reduction

At each measurement location, a predetermined number of simultaneous instantaneous velocity components were recorded. The velocity measurements result from signals scattered by a random distribution of particles in the gas that travel through the probe volume. Long and short clock counts are also recorded. When an unsatisfactory measurement was taken for either velocity component, an aperiodicity failure resulted. The final number of velocities, N, that was used in data reduction equaled the number of measurements taken simultaneously without aperiodicity failures. The mean velocity, $\bar{u}$, is determined for each set of N samples by:

$$\bar{u} = \frac{1}{N} \sum_{i=1}^{N} u_i, \tag{11}$$

where u_i is the instantaneous velocity for one measurement of the sample set. The velocity variance, $\overline{u'^2}$ for the sample set is:

$$\overline{u'^2} = \frac{1}{N-1} \sum_{i=1}^{N} (u_i - \bar{u})^2. \tag{12}$$

The standard deviation, σ, is the square root of the velocity variance. The local turbulence intensity is defined as σ/u and the reference turbulence intensity is defined as σ/V where V is the velocity of the flow at a preselected point of the flow.

The cross correlation, $\overline{u'v'}$, of the sample distribution is given by:

$$\overline{u'v'} = \frac{1}{N} \sum_{i=1}^{N} (u_i - \bar{u})(v_i - \bar{v}), \tag{13}$$

where u_i and v_i are simultaneous orthogonal velocity components.

The skew, or third moment, S, of the sample distribution is given by:

$$S = \frac{1}{N\sigma^3} \sum_{i=1}^{N} (u_i - \bar{u})^3 \tag{14}$$

Finally, the Kurtosis, or fourth moment, β, of the sample distribution is given by:

$$\beta = \frac{1}{N\sigma^4} \sum_{i=1}^{N} (u_i - \bar{u})^4. \tag{15}$$

The third moment is used to determine if the sample distribution is skewed positively or negatively. The fourth moment is used to determine the "flatness" of the sample distribution. For a normal distribution, $S = 0$ and $\beta = 3$. When a velocity measurement causes either the third or fourth moment to deviate considerably from the values for a normal distribution, that velocity measurement is not used in the data analysis process.

2.6 Laser Velocimeter Measurement Precision

Several variables affect the precision of the laser velocimeter system. They include the sample size, the zero crossing detector trigger level, the fringe spacing, the reference frequency, and the low pass filter setting. The sample size was made as large as possible to increase the accuracy of the mean and standard deviation. The tolerance of the mean velocity, $Tol(\bar{u})$, is defined as:

$$Tol(\bar{u}) = \bar{Z} \times \sigma_{\bar{u}} \tag{16}$$

where $\bar{Z}$ is determined by the confidence level of the measurement and $\sigma_{\bar{u}}$ is the standard deviation of the mean given by:

$$\sigma_{\bar{u}} = \sigma/N^{1/2}. \tag{17}$$

Equations (16) and (17) can be combined to give:

$$\mathrm{Tol}(\bar{u}) = \bar{Z}\sigma/N^{1/2}. \tag{18}$$

The tolerance of the calculated turbulence velocity, u', is given by [5]:

$$\frac{\mathrm{Tol}(u')}{u'} = \bar{Z}[\frac{1}{4N}(\beta - \frac{N-3}{N-1})]^{1/2}. \tag{19}$$

The confidence level, $\bar{Z}$, determines the probability that the calculated value of the mean velocity, $\bar{u}$, is within the range of $\bar{u} \pm \mathrm{Tol}(u)$. For $\bar{Z}=1$, the probability is 68%. For $\bar{Z}=2$, it is 95% and for $\bar{Z}=3$, it is 98%. From the preliminary data, nominal values of $\bar{Z} = 2$ (95 percent confidence), $\sigma = 1.40$ m/s, N = 1300, and $\beta = 4$ were determined to give tolerances of $\mathrm{Tol}(\bar{u}) = 0.08$ m/s (0.26 ft/s) from equation (18) and Tol(u')/u' = 0.048 or 4.8 percent of u' from equation (19).

For this experiment, a sample size of 1500 was used to provide adequate tolerances. Out of these 1500 velocity measurements, usually more than 1300 were acceptable for data reduction. To record a sample size this large for each point of measurement required that the LV microprocessor be connected to a computer with a large enough memory to perform the data storage and reduction. This was accomplished by linking the LV microcomputer at the test site to a Data General S-230 computer with hard disk storage at the CFFF.

The zero crossing detector trigger level is set to maximize the number of acceptable velocity readings within a reasonable acquisition time. The acquisition time is the number of seconds required to take 1500 sample points. The zero crossing detector is set by trial-and-error while observing the raw and processed signals on an oscilloscope. The fringe spacing is adjusted by varying the angle between the intersecting beams at the probe volume with the focusing optics. Increasing this angle shortens the probe volume which is beneficial because the location at which velocity measurements are taken is more precise. On the other hand, increasing the beam angle increases the signal frequencies, decreasing the resolution of the LV processor. Therefore, the fringe spacing is set to provide adequate processor resolution.

The fringe spacing is measured in the following manner: the probe volume is focused on a plane surface and then the probe volume is moved inward by a distance, L. With the probe volume at this location, the horizontal spacing, H, between the beams, and the vertical spacing, V, between the beams are measured. Knowing these variables, the fringe spacings, δx and δy can be determined using geometric formulas [6]:

$$\delta_x = 0.2573 \left(1 + \frac{4L^2}{H^2}\right)^{1/2}, \tag{20}$$

$$\delta_y = \delta_x \times \frac{H}{V} . \tag{21}$$

Fringe spacings were calculated for 20 different values of L so that mean values of δ_x and δ_y could be determined. The mean values were 38.01 ± 2.08 microns for δ_x and 22.81 ± 0.67 microns for δ_y.

The minimum measurable signal frequency depends on the probe volume diameter, D_o, the maximum flow velocity, U_{max}, and the minimum number of signal cycles, N_o, required by the signal processor. The probe volume diameter, D_o, is defined by:

$$D_o = \frac{4F\lambda}{\pi D \cos \theta/2} \tag{22}$$

where F is the focal length of the transmitting lens and D is the beam diameter at the transmitting lens. For this case F = 0.705 m (27.75 in), $\lambda = 5.145 \times 10^{-7}$ m, D = 5 mm (0.20 in), and $\cos \theta/2 = 1$. Using these values, the probe volume diameter was found to be 92.35×10^{-6} m. The maximum flow velocity magnitude in the superheater model was estimated to be 7.62 m/s (25 ft/s) in the direction of the flow or the positive X-direction. The maximum velocity magnitude in the negative X-direction and in both transverse directions was estimated to be 3.05 m/s (10 ft/s). The minimum detectable LV signal frequency is given by:

$$f_{min} = \frac{N_o \,|\, U_{max} \,|}{D_o} . \tag{23}$$

The maximum signal frequency, f_{max}, is the low pass filter setting. The possible settings for the low pass filter are 100, 200, and 500 KHz, 1, 2, and 5 MHz. The low pass filter is set at the lowest possible frequency that will allow the full range of velocities to be measured thus minimizing signal noise. The value of f_{max} is given by:

$$f_{max} = f_{min} + \frac{|U_{max}|}{\delta} + \frac{|U_{min}|}{\delta} \tag{24}$$

while the Bragg reference frequency is given by:

$$f_o = f_{min} + \frac{|U_{min}|}{\delta} . \tag{25}$$

2.7 Test Procedures

2.7.1 Setting experimental flow rate.

Before any data was taken, the bulk flow rate at the entrance of the ash-seed hopper section was set at approximately 1200 CFM to create the same Reynolds number in the superheater model as in the CFFF superheater. The flow rate was measured with a pitot tube and a manometer. The pitot tube was traversed horizontally and vertically across the cross sectional area of the ash-seed hopper section in increments such that flow velocity was measured at the center of eight equal areas. The bulk flow rate was then determined by taking the average value of these eight velocities. The flow rate was adjusted with a variable speed pulley on the motor shaft of the backwardly-inclined centrifugal fan and additional measurements were made. The fan was adjusted until a bulk flow rate of approximately 1200 CFM was achieved.

2.7.2 Establishment of coordinate system for LV probe volume and seeding.

Before each test run, the laser velocimeter probe volume was focused on the wall of the model and the position indicator was set to the correct value in all three dimensions. Seeding with water particles was accomplished with a water spray nozzle located far upstream at the air inlet. The seeding rate of microscopic mist particles was varied by adjusting the spray nozzle air pressure or water pressure to obtain the best output signal from the LV on an oscilloscope. Model testing was done at night because the air during the day was not saturated, causing a high percent of the water particles to evaporate before they reached the probe volume. Also, it was found that atmospheric air is more uniform in temperature and relative humidity at night.

2.7.3 Data acquisition sequence. Velocity measurements were taken at various locations in increments of 12 mm (0.2292 in) in the X-direction from the inlet transition section to the end of Test Section 2 and in increments of 12 mm (0.2292 in) in the Z-direction from the centerline of the model to 9.53 mm (3/8 in) from the inner wall of the model. From the inlet transition to the entrance of the cooling section, velocity measurements at these points were taken at different Y-planes in the model. Data on cross sectional grids was taken in the inlet transition, at the entrance of Test Section 1, between the last row of cooling tubes and the first row of steam tubes, in Test Section 1, at the entrance of the cooling section, and in front of the steam tubes in Test Section 2.

3.0 RESULTS AND DISCUSSION

3.1 Coordinate System for Data Reduction

The laser beams passed into the model and scattered light passed out of the model through the top wall in each section of the superheater model. An illustration of the top wall and the SHTM tube arrangement is shown in Figure 9, page 48. The coordinate system for data acquisition was as follows: the Y-Z plane origin (Y = 0.0, Z = 0.0) is the exact center of the rectangular cross section of the model with Z being the direction perpendicular to the side walls with a range of -5.875 inches to +5.875 inches inside the model. The Y-direction is perpendicular to the top and bottom walls of the model with a range of -11.875 inches (top wall) to +20.375 inches (bottom of ash-seed hoppers). The X-direction is the direction of the flow with the origin (X = 0.0) located at the beginning of Test Section 1.

3.2 Introduction to the Measurements and Data Displays

Results from the model testing are plotted in Figures 10 through 25, pages 49 to 64. Each plot shows a flow pattern made up of velocity vectors. The length of each vector represents the magnitude of the velocity at one location. Each velocity vector origin is at the point of velocity measurement. The geometric configuration is identical from Z =0.0 to each sidewall, which should result in a symmetrical flow with respect to the centerplane (Z = 0.0). This was verified by experiment with the data shown in Figures 20 and 21, pages 59 and 60. For this reason, the majority of data were only taken on one side of the plane of symmetry (Z = 0.0). Figures 10 through 12 pages 49 through 51, show the velocity field in the X-direction at different X-Z planes in the inlet transition, Test Section 1, and the cooling section entrance. These three figures show the velocity fields at Y = 6.0 inches (toward the top wall), Y = 0.0 inches (in the middle of the superheater model), and Y = -6.0 inches (toward the bottom). Figures 13 through 17, pages 52 through 56, are plots of mean velocity and turbulence intensity versus distance in the X-direction in different X-Y planes. For each plot, an X-Z plane is represented at Y = 6.0 inches, Y = 0.0 inches, and Y = -6.0 inches. Figure 18, page 57, shows the velocity field in the cooling section. Figure 19, page 58, shows the velocity field at the end of the cooling section and in Test Section 2. Figure 20, page 59, shows a cross-sectional profile of the mean velocities and turbulence intensities in the inlet transition at X = -7.5 inches. Figure 21, page 60, shows a cross-sectional velocity field in the inlet transition at X = - 7.5 inches. Figures 22 through 25, pages 61 through 64, show cross-sectional profiles of mean velocities and turbulence intensities in different Y-Z planes throughout the model. Figure 22, page 61, shows a cross-sectional plane directly in front of the cooling tubes in Test Section 1 at X = -0.521 inches. Figure 23, page 62, shows the cross-sectional profile between the cooling tubes and steam tubes in Test Section 1 at X = 9.042 inches. Figure 24, page 63, shows the cross-sectional profile at the cooling section entrance at X = 17.208 inches. Figure 25, page 64, shows the cross-sectional profile in front of the steam tubes in Test Section 2 at X = 53.957 inches.

3.3 Discussion of the Measurements

The velocity field in Figure 10, page 49, shows that the incoming flow near the top wall in the inlet transition is almost at zero velocity. However, flow wells up from the bottom of the inlet section so that the axial velocity increases to about 1 m/s before the flow reaches the cooling tubes in Test Section 1. The velocity field in Figure 11, page 50, shows that the flow in the X-Z plane which is half-way down the SHTM, has a more uniform velocity through the inlet transition in the X-direction but the flow axial velocity tends to be higher near the side walls of the model than at the centerline (Z = 0.0 inches). The flow near the bottom of the SHTM, shown in Figure 12, page 51, has the same characteristics as the flow half-way down the SHTM but at a higher axial velocity. The flow near the top wall at Y = 6.0 inches was unaffected by the side walls because of the low velocity of the flow.

The cross-sectional profile of the inlet transition shown in Figure 20, page 59, shows a rapid flow near the bottom wall and a reversed flow near the top wall of the inlet transition. This recirculation in the inlet transition is caused by the flow turning 90° as the gas travels from the ash-seed hopper into the inlet transition. Near the bottom of the inlet transition, the flow is uniform across the X-Y plane and the turbulence intensity is very small. Near the centerline (Y = 0.0 inches), the velocity of the flow is higher near the side walls than near the center (Z = 0.0 inches). The turbulence intensity is higher in the top section of the inlet transition than in the bottom section because of the recirculation and reverse flow existing in the top section of the inlet transition. The velocity field in Figure 21, page 60, shows the mean velocities in the flow throughout the inlet transition and corresponds with Figure 20, page 59. Figures 20 and 21, pages 59 and 60, show the symmetry on both sides of the centerline (Z = 0.0 inches) which allowed data to be taken in half of the Y-Z plane during the remainder of the model testing. Figure 22, page 61, shows a cross-sectional plane directly in front of the cooling tubes in Test Section 1 at X = -0.521 inches. This plot shows that the gas is still in recirculation as it enters Test Section 1. This plot verifies what was seen in Figures 11 and 12, pages 50 and 51, in that the flow velocity is higher near the side wall than near the centerline (Z = 0.0 inches) in the bottom half of the inlet transition. The flow is reversed near the top wall of the model. The gas flow velocity is higher as the flow approaches the bottom of the model. The turbulence intensity is generally uniform throughout the cross-sectional plane. Figure 23, page 62, shows a cross-sectional plane between the last row of cooling tubes and first row of steam tubes in Test Section 1 at X = 9.042 inches. There is a large variation of velocity as the gas travels between the tubes. The turbulence intensity is highest in the wake of the tubes behind each tube row. The flow velocity is highest near the bottom of the model. When the gas reaches a row of cooling tubes, as in Test Section 1, the flow area is reduced by approximately 42% by tube area blockage. This causes the velocity of the flow to increase by a factor of 1.7 through the plane of the tube row. When the gas reaches a row of steam tubes which are smaller in diameter, the flow area is reduced by approximately 25%. This causes the velocity of the flow to increase by a factor of 1.3 which also causes flow acceleration in the plane of the steam tube rows. Recirculation or a wake occurs behind each tube in the flow. For higher velocity inlet flow, the recirculation or wake increases behind the tubes. For this reason, there is a much higher amount of recirculation or larger wakes behind the tubes near the bottom of the model than near the top wall. Throughout Test Section 1, the velocity of the gas is higher between the outer tube and the side wall than in between the inner or central tubes. Almost immediately after the gas passes out of the region containing tubes in Test Section 1, the effect of the tubes on the flow disappears as the flow pattern is becoming uniform. The velocity is still greater near the side wall; however, and near both the top and bottom walls than at the center (Y = 0.0 inches).

Plots of mean velocity and turbulence intensity versus distance through the model are shown in Figures 13 through 17, pages 52 through 56, in different X-Y planes. For each plot, an X-Z plane is represented for Y = 6.0 inches (near the top wall), Y = 0.0 inches (center of the model), and Y = -6.0 inches (near the bottom). These plots show that the gas velocity becomes uniform across the X-Z plane as the gas travels through the superheater. The gas flow takes longer to become uniform near the side wall (Z = -5.5 inches). The axial velocity increases as the gas flows between the tubes and then returns to lower, near mass average values, between the tube rows. The turbulence intensity is highest between the tube rows because of the recirculation or wake behind each tube. As the gas travels through the cooling section, the flow velocity increases and then decreases as it passes into and out of the tube rows. From Z = 0.0 inches to Z = -4.125 inches, the velocity patterns for the three values of Y are very similar. Thus there is vertical similarity except for the magnitudes of the velocities. In the X-Y plane where Z = -5.5 inches, there is little fluctuation in the mean velocity at Y = 6.0 inches, but at Y = 0.0 inches and Y = -6.0 inches, there is a much larger variation of both mean velocity and turbulence intensity, especially near the bottom of the model at Y = -6.0 inches.

Figure 18, page 57, shows the velocity field through the cooling section. Figures 13 through 17, pages 52 through 56, show that the flow is now uniform across the Y-Z plane by this axial distance. Therefore, the flow field shown in Figure 18, page 57, is representative of the more uniform flow in this part of the model. The data results show that the flow around each row of tubes after the first row is identical. The bulk velocity of the gas does not vary significantly as the gas travels through the cooling section. Figure 19, page 58, shows the velocity field in the cooling section exit and in Test Section 2. When the gas leaves the cooling section, the wakes of the tubes disappear rapidly so that the gas flow becomes uniform.

Throughout the model, the gas velocity is higher near the side wall than at the centerline (Z = 0.0 inches). The region of this higher velocity is generally between Z = -5.00 inches and Z = -5.875 inches. Thus, the effects of inlet flow nonuniformity do persist in some aspects through the first section of the SHTM.

Figure 24, page 63, shows a cross-sectional plane at the cooling section entrance at X = 17.208 inches. The flow is now uniform in the Y-direction except near the side wall where the gas velocity is higher near the bottom of the model. The turbulence intensities are uniform in the Y-direction. A cross-sectional plane in front of the steam tubes in Test Section 2 at X = 53.957 inches is shown in Figure 25, page 64. In this region, the flow is uniform in the Y-direction except near the bottom of the model where the flow velocity is higher on the centerline (Z = 0.0 inches) than near the side wall. In all the previous sections of the model, the flow velocity was higher near the side wall than at the centerline (Z = 0.0 inches). This change may have occurred for several reasons including the effect of the open area above the ash-seed hopper cavity in front of the steam tubes in Test Section 2, or because of a swirl component of the bulk flow caused by the nonuniform inlet conditions.

3.4 Analysis of Vortex Shedding and Flow Stability

A time series analysis was accomplished by computer to determine if any periodic or random flow oscillations occur in the superheater. The computer analysis showed that periodic flow oscillations occur in the area behind each cooling section tube with a frequency between 4 and 5 Hertz. These periodic flow oscillations are caused by vortex shedding behind the tubes. The analysis also showed that there are no significant flow oscillations behind the steam tubes and that the periodic flow oscillations behind the cooling section tubes quickly damp out after the gas passes through a row of tubes.

3.5 Effects of the Flow Patterns on SHTM Heat Transfer

Total heat transfer per unit length was calculated for each group of tubes or tube bundle using the following equations [7]: First, the maximum velocity, V_{max}, is calculated by:

$$V_{max} = \frac{V_{\infty}a}{a-D} \tag{26}$$

where a is the cross-sectional spacing between the tubes, D is the outside tube diameter, and V_{∞} is the bulk velocity of the flow entering the tube bundle region. Next, the maximum Reynolds number is calculated by:

$$Re_{max} = \frac{V_{max}D}{\nu_g} \tag{27}$$

where ν_g is the kinematic viscosity of the gas. Next, the overall heat transfer coefficient, h, is given by:

$$h = \frac{K_g}{D} C_1(Re_{max})^n \tag{28}$$

where K_g is the thermal conductivity of the gas. C_1 and n are constants that depend on the tube diameter, D, the longitudinal spacing, b, and the cross-sectional spacing, a. C_1 and n were found in a tube bundle heat transfer table developed by E. D. Grissom [7]. Finally, the total heat transfer per unit length of the tube bundle, q/L is given by:

$$q/L = h\pi DN(T_s - T_{\infty}) \tag{29}$$

where N is the total number of tubes, T_s is the temperature of the tube surface, and T_{∞} is the bulk temperature of the gas. For the bundle of cooling tubes in Test Section 1, q/L was calculated for three X-Z planes because the velocity entering the tube bundle is different in each plane. The total heat transfer per unit length was also calculated for an individual tube in the bundle. The results of the heat transfer calculations are given in Table 2.

3.6 Ash Deposition Characteristics Affected by Flow Patterns

Ash deposition occurs when an ash particle strikes the tube surface and adheres to it because of the impact. The greater the velocity of the flow, the more likely this is to occur. In a row of cooling tubes, the tubes occupy 42% of the cross-sectional area which implies that up to 42% of the ash particles in the flow will strike a cooling tube. For a row of steam tubes, the tubes occupy 25% of the cross-sectional area which implies that up to 25% of the ash particles in the flow will strike a steam tube. Ash deposition is also increased by high turbulence intensity in the flow. Ash deposition caused by the direct impact of ash particles carried to the tubes by the mean velocity occurs more than ash deposition caused by high turbulence intensity [8]. Ash deposition occurs much more frequently on the front of tubes than on the back of the tubes.

3.7 Effect of SHTM Flow on Erosion Characteristics

Tube erosion occurs when many particles strike the tube surface over a period of time and cause the surface to wear away. In the superheater model study, it was found that the velocity of the flow is not high enough to cause a significant amount of erosion.

Table 2. Heat Transfer Rates in the SHTM.

Location	Tube Bundle (Btu/hr• ft)	Per Tube (Btu/hr• ft)
TS1 cooling tubes at Y = 6.0 inches (near top wall)	2.15×10^5	6.73×10^3
TS1 cooling tubes at Y = 0.0 inches (center)	3.88×10^5	1.21×10^4
TS1 cooling tubes at Y = 6.0 inches (near bottom)	4.39×10^5	1.37×10^4
TS1 steam tubes	6.68×10^4	4.18×10^3
Cooling section	8.90×10^5	9.27×10^3
TS2 steam tubes	3.18×10^4	1.99×10^3

4.0 SUMMARY AND CONCLUSIONS

4.1 Summary

The isothermal velocity flow field survey of the superheater model can be summarized as follows:

1. The 90° turn of the flow as the gas travels from the ash-seed hopper into the inlet transition causes a large amount of recirculation on the top plane of the inlet transition, which in turn causes the flow entering the superheater to be much faster near the bottom of the model than near the top.
2. The flow velocity is generally higher near the sidewalls than near the centerline (Z = 0.0 inches).
3. The axial velocity of the flow increases by a factor of 1.7 when the gas passes between a row of cooling tubes and by a factor of 1.3 when the gas passes between a row of steam tubes.
4. The highest turbulence intensities occur behind each tube row, especially between tube rows that are closely spaced.
5. The ash-seed hopper cavities at the bottom of each superheater section do not have a significant effect on the gas flow.
6. Recirculation or a wake occurs behind each tube in the gas flow. The higher the velocity of the gas, the larger the wake is.

7. Almost immediately after the gas passes out of an area containing tubes, the effect of the tubes on the flow disappears and the flow tends toward uniformity.

4.2 Conclusions

The following conclusions can be drawn from the superheater model study:

1. The recirculation in the inlet transition due to the geometric configuration of the ash-seed hopper and inlet transition reduces the efficiency of the superheater because of the reduction of heat transfer due to insufficient flow velocity in the top section of Test Section 1. Ash deposition is expected to be increased in the bottom section due to excessive flow velocity and in the top section due to higher turbulence intensity.
2. The flow across the Y-Z plane becomes uniform before it reaches the cooling section.
3. Ash deposition rates are expected to be highest in the front row of tubes in each section where the most particles strike the tube surface, where mean velocities are highest, and where turbulence velocities are the highest.
4. Periodic flow oscillations occur behind the cooling section tubes due to vortex shedding. These periodic flow oscillations damp out quickly after the gas passes between a row of cooling tubes. There are no significant flow oscillations behind the steam tubes.

5. Velocities of the gas flow in the SHTM are not high enough anywhere in the SHTM to induce any significant amount of erosion.

5.0 RECOMMENDATIONS FOR SHTM MODIFICATIONS

Based on the conclusions drawn from the superheater model study, the following recommendations for improving the efficiency of the superheater can be made:

1) The anticipated nonuniform ash deposition and heat transfer in Test Section 1 caused by the recirculation in the inlet transition can be eliminated by one of these three methods:

   A. Change the ash-seed hopper and inlet transition configuration to produce a smoother flow into the inlet transition so that the gas flow is more uniform when it reaches Test Section 1.

   B. Increase the length of the inlet transition so that the flow is uniform before it reaches Test Section 1. This would also allow more particles to fall to the bottom before they reach Test Section 1.

   C. Install a flow straightener at the inlet transition entrance. The flow straightener would have to be made from a material that can withstand a temperature of 2300°F.

2) Increase the distance between the last row of cooling tubes and the first row of steam tubes in Test Section 1 to reduce the turbulence velocity in this region and thus reduce ash deposition.

3) Sootblowers should be operated in front of each section of tubes and between the cooling tubes and steam tubes in Test Section 1 to reduce ash deposition.

These recommendations should be incorporated only if they are cost effective. They could also be beneficial in the design of future MHD steam generation systems.

LIST OF REFERENCES

LIST OF REFERENCES

1. J. B. Heywood, G. T. Womack, Open Cycle MHD Generation, Pergamon Press, 1969.

2. T. C. Shaver, J. P. Foote, D. Gonzalez, M. K. White, "LMF3 Test Plan for the Low Mass Flow Test Train at the Coal Fired Flow Facility," The University of Tennessee Space Institute, Tullahoma, Tennessee, February 1984.

3. R. D. Groff, W. T. McMinn, J. Foote, "Final Design Report for the Low Mass Flow Coal Fired Flow Facility Superheater Module," The University of Tennessee Space Institute, Tullahoma, Tennessee.

4. William Bober, Richard A. Kenyon, Fluid Mechanics, pp. 250-292, John Wiley and Sons, Inc., 1980.

5. V. A. Cline, H. T. Bentley, "Application of a Dual Beam Laser Velocimeter to Turbulent Flow Measurements," Arnold Engineering Development Center, Air Force Systems Command, Arnold Air Force Station, Tennessee, September 1974.

6. D. O. Barnett, T. V. Giel, Jr., "Application of a Two-Component Bragg-Diffracted Laser Velocimeter to Turbulence Measurements in a Subsonic Jet," Arnold Engineering Development Center, Air Force Systems Command, Arnold Air Force Station, Tennessee, May 1976.

7. D. R. Pitts, L. E. Sissom, Theory and Problems of Heat Transfer, McGraw-Hill Book Company, 1977.

8. M. K. White, "Superheater Gas-side Fouling and Corrosion," HRSR Presentation, The University of Tennessee Space Institute, Tullahoma, Tennessee, May 1985.

APPENDIX

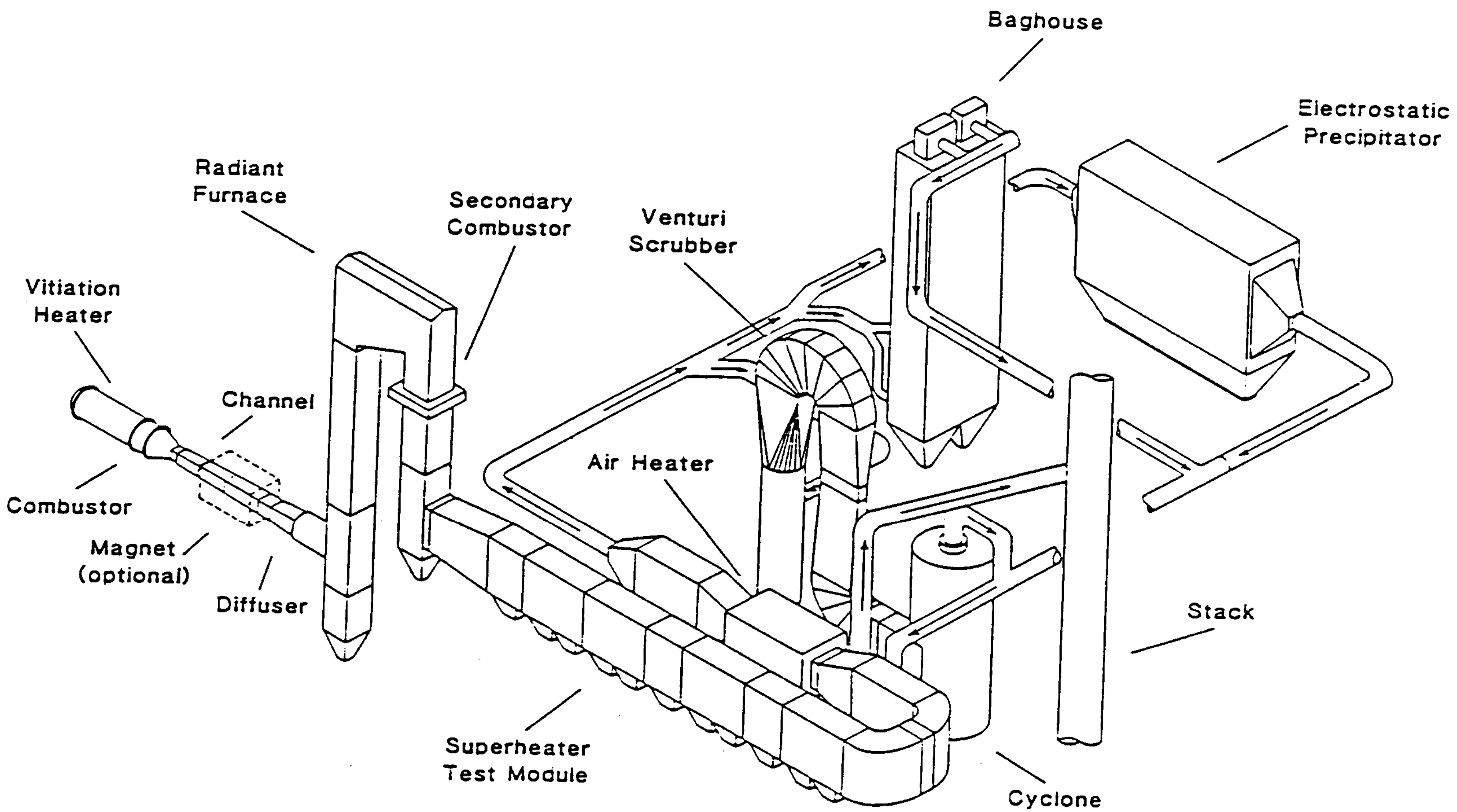

Figure 1. CFFF Low Mass Flow Train.

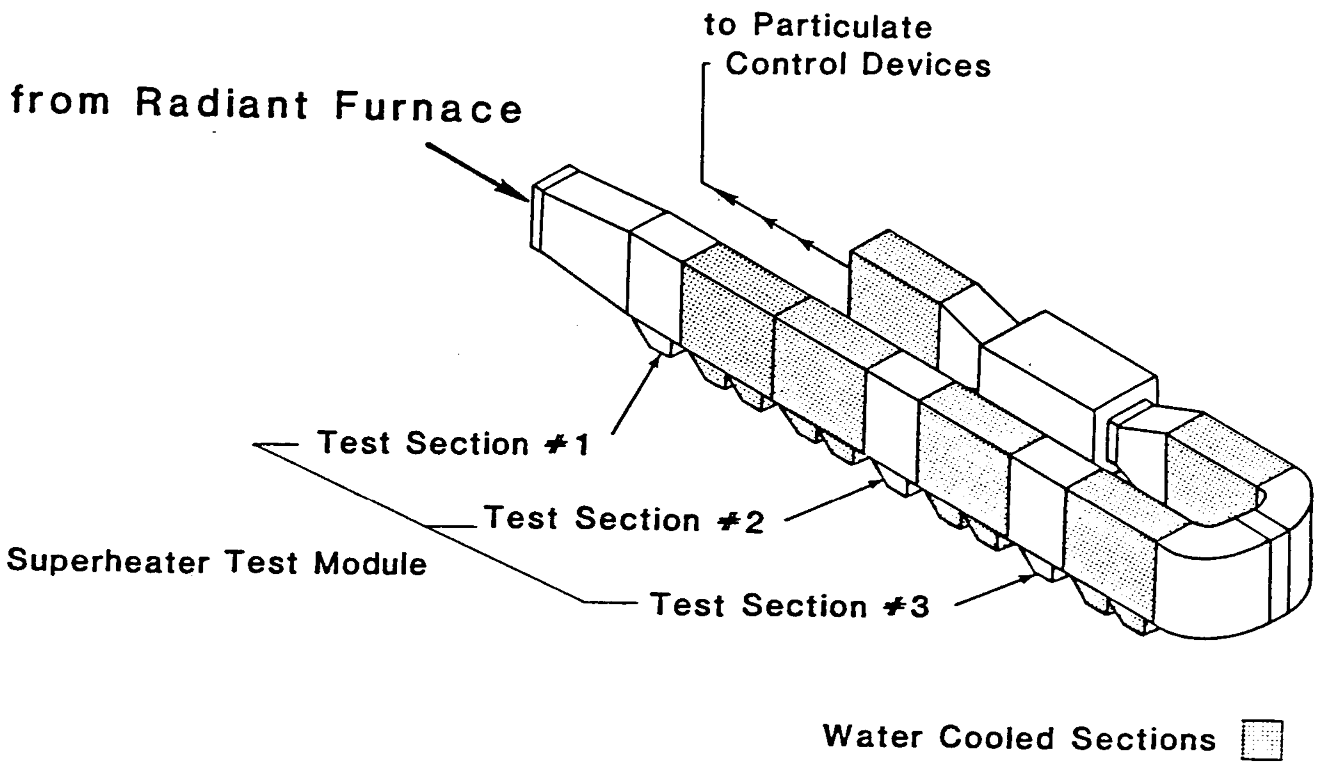

Figure 2. CFFF Superheater Test Module Arrangement.

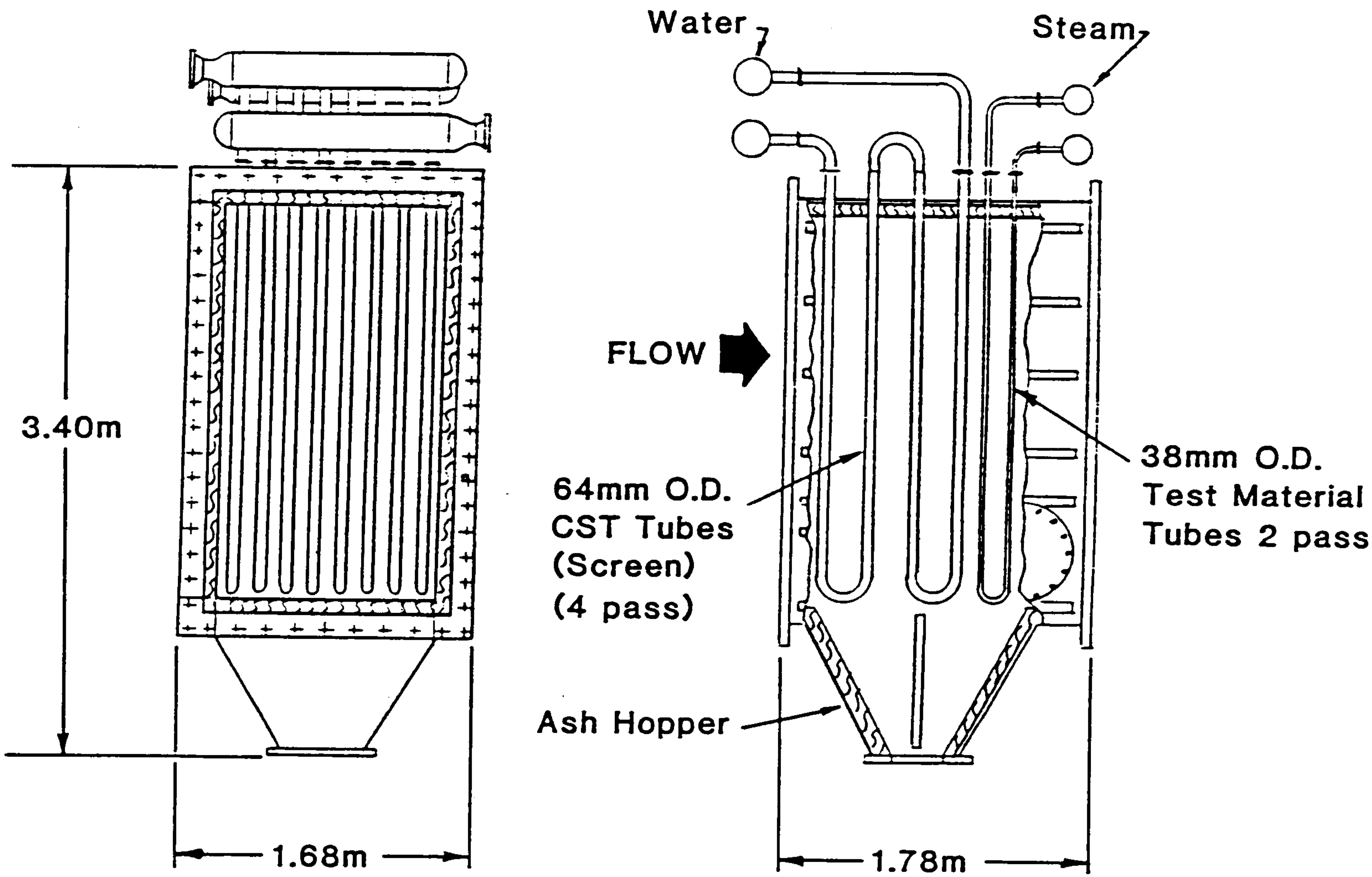

Figure 3. SHTM Test Section 1.

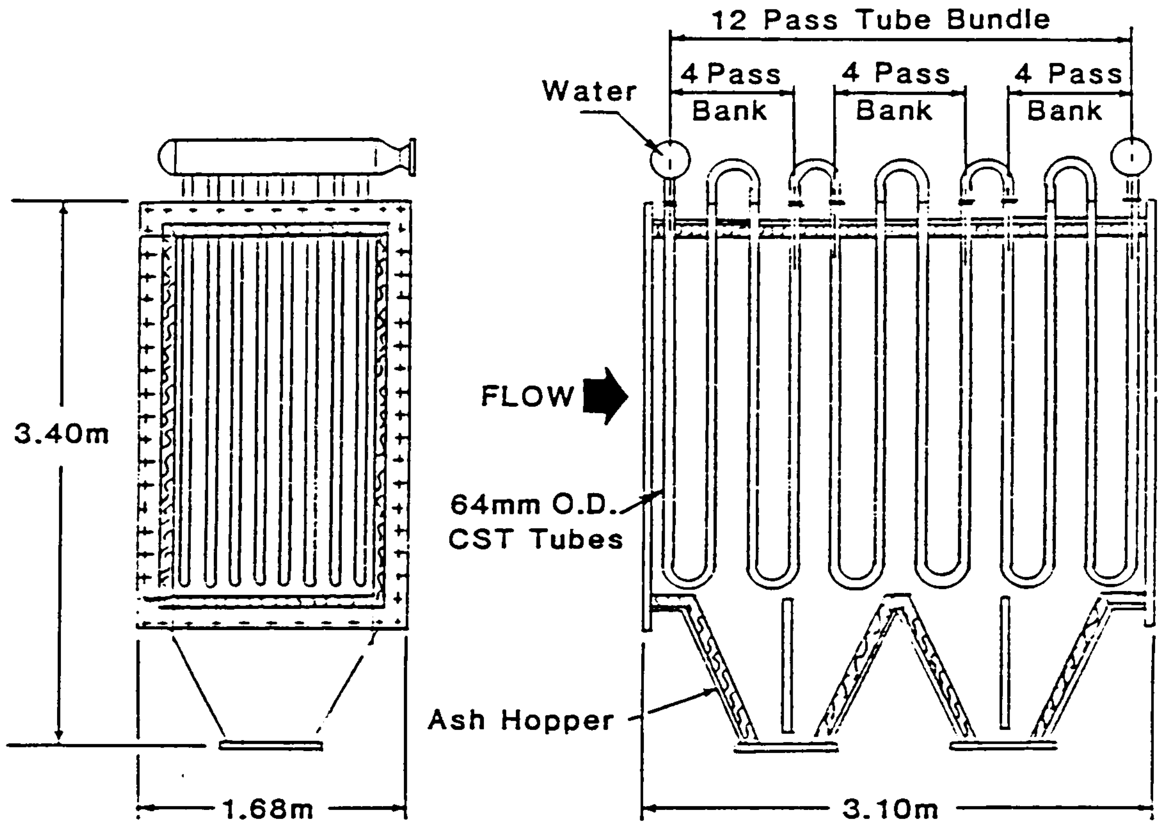

Figure 4. SHTM Cooling Section.

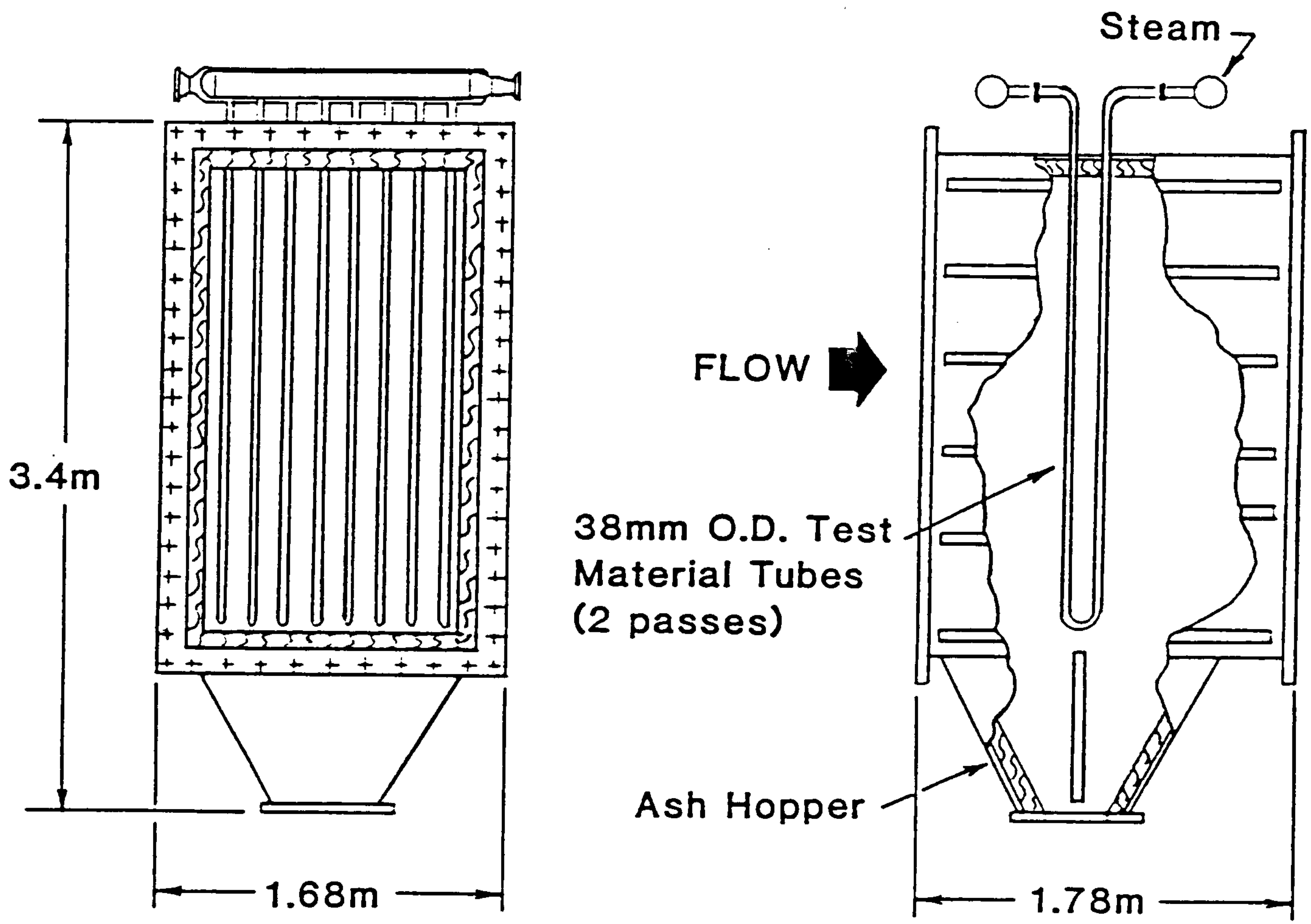

Figure 5. SHTM Test Section 2.

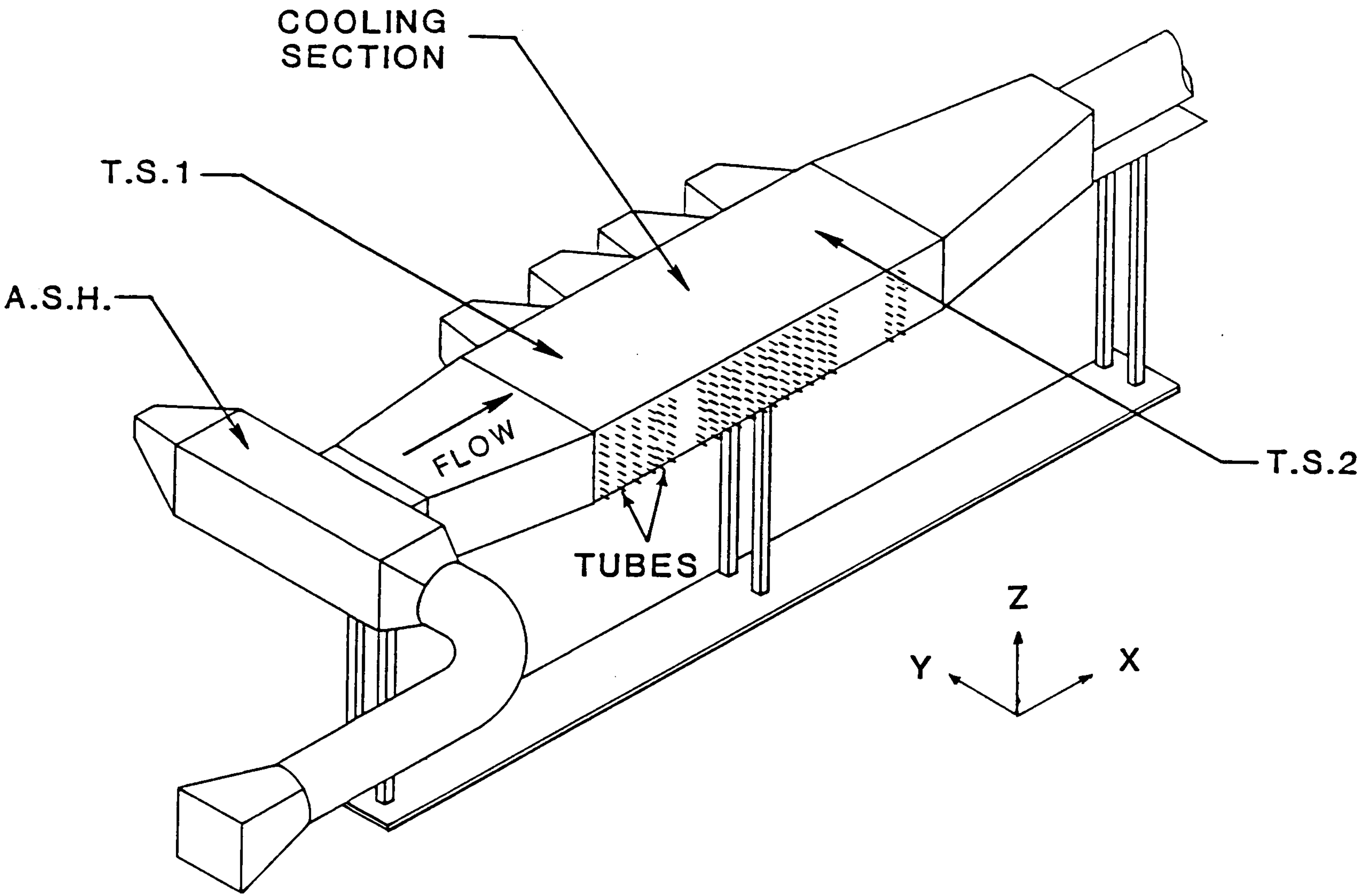

Figure 6. Superheater Model.

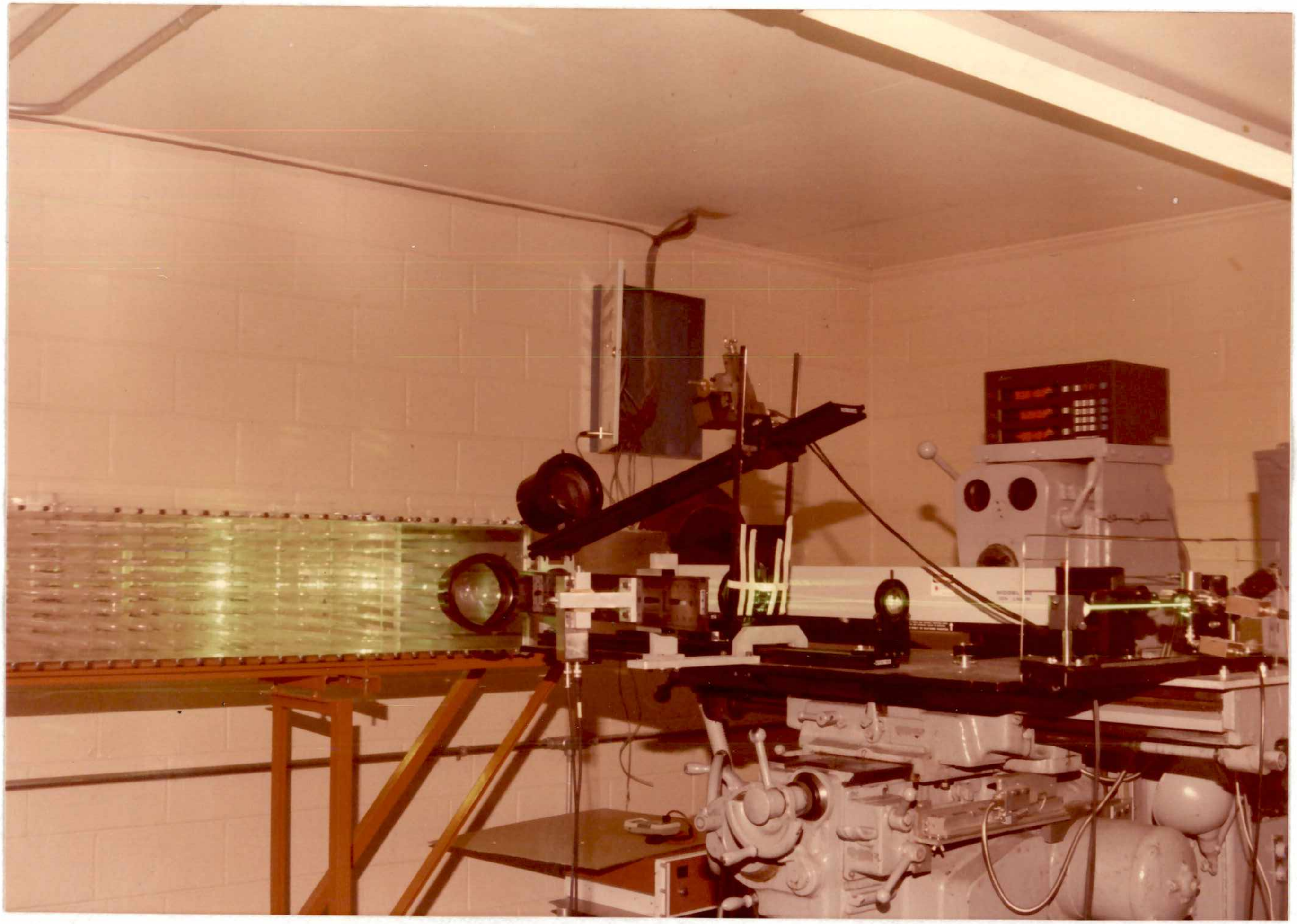

Figure 7. Superheater Model and Laser Velocimeter System.

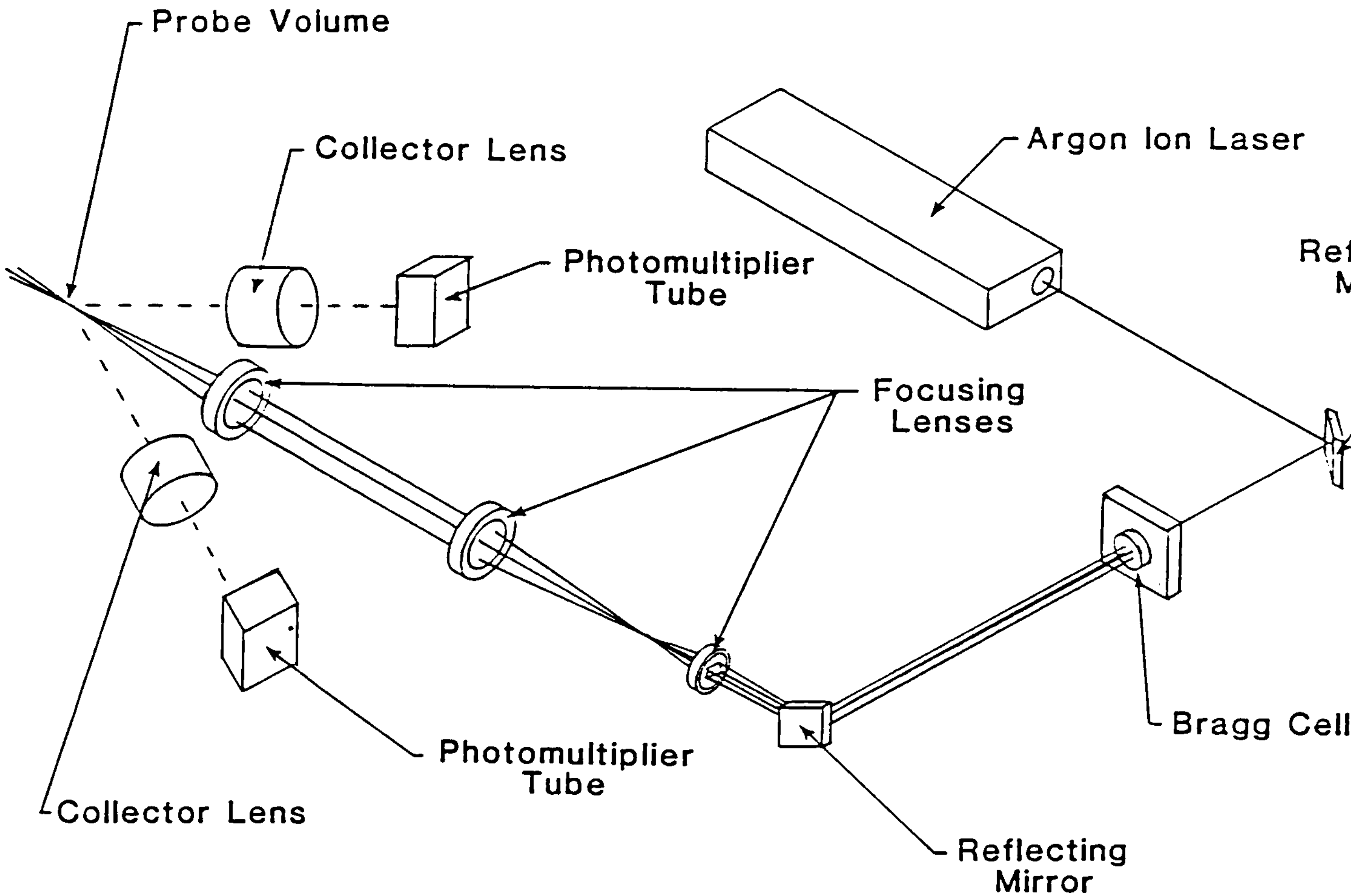

Figure 8. Diagram of Laser Velocimeter System.

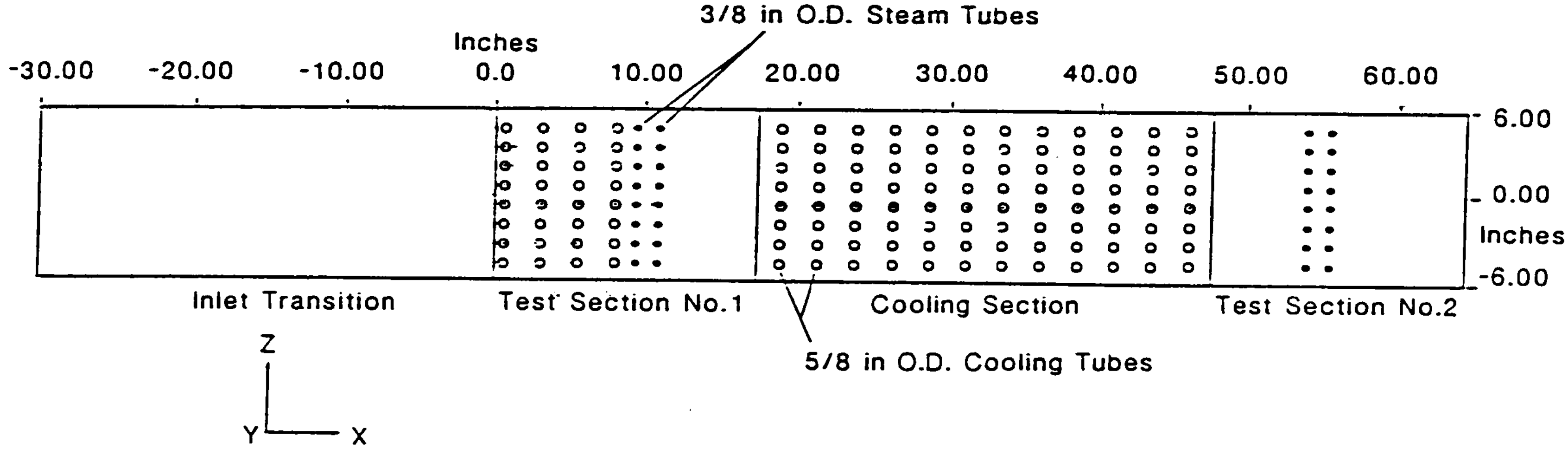

Figure 9. Superheater Model Tube Arrangement.

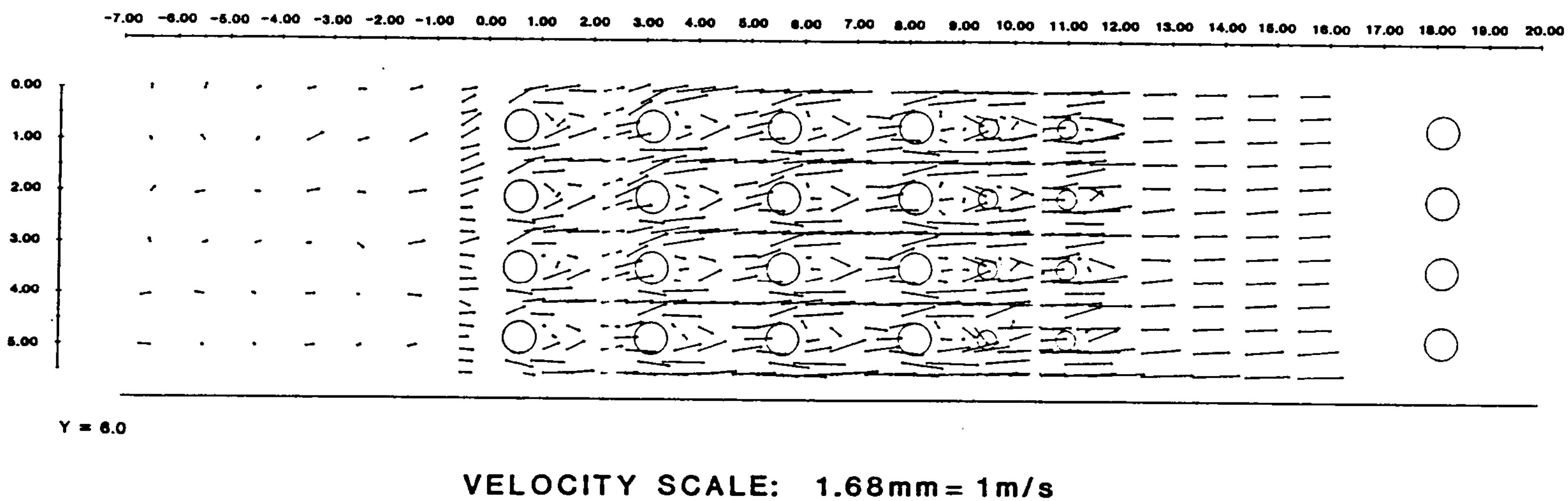

Figure 10. Velocity Field in the Inlet Transition, Test Section 1, and Cooling Section Entrance at Y = 6.0 inches (near the top of SHTM).

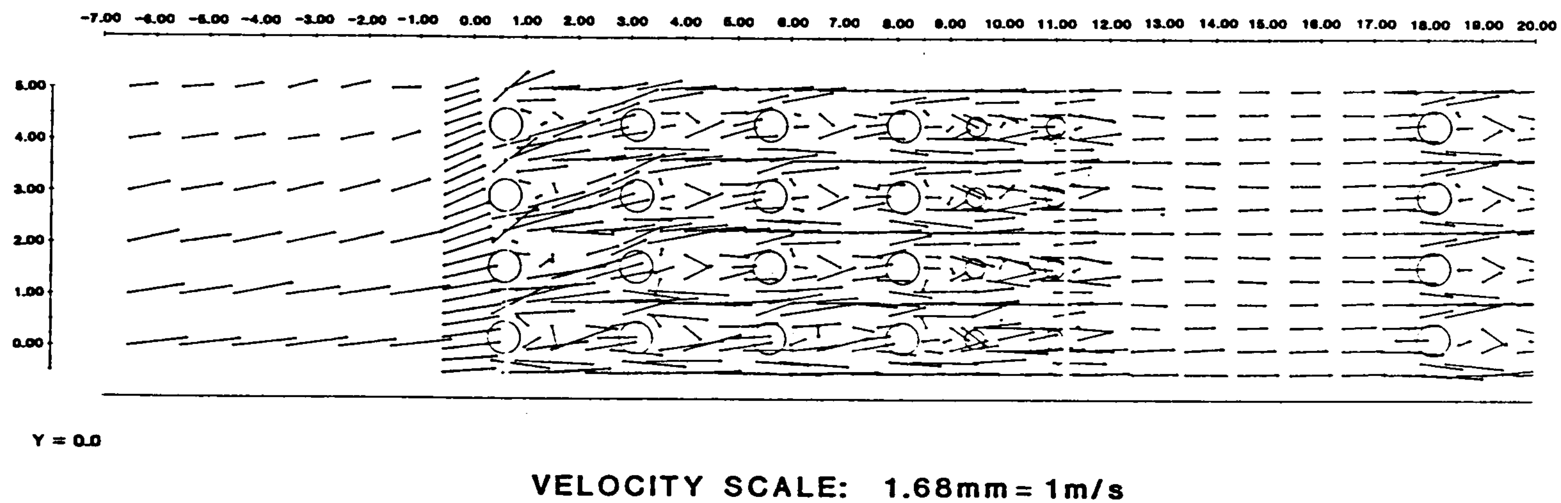

Figure 11. Velocity Field in the Inlet Transition, Test Section 1, and the Cooling Section Entrance at Y = 0.0 inches, (in the middle of SHTM).

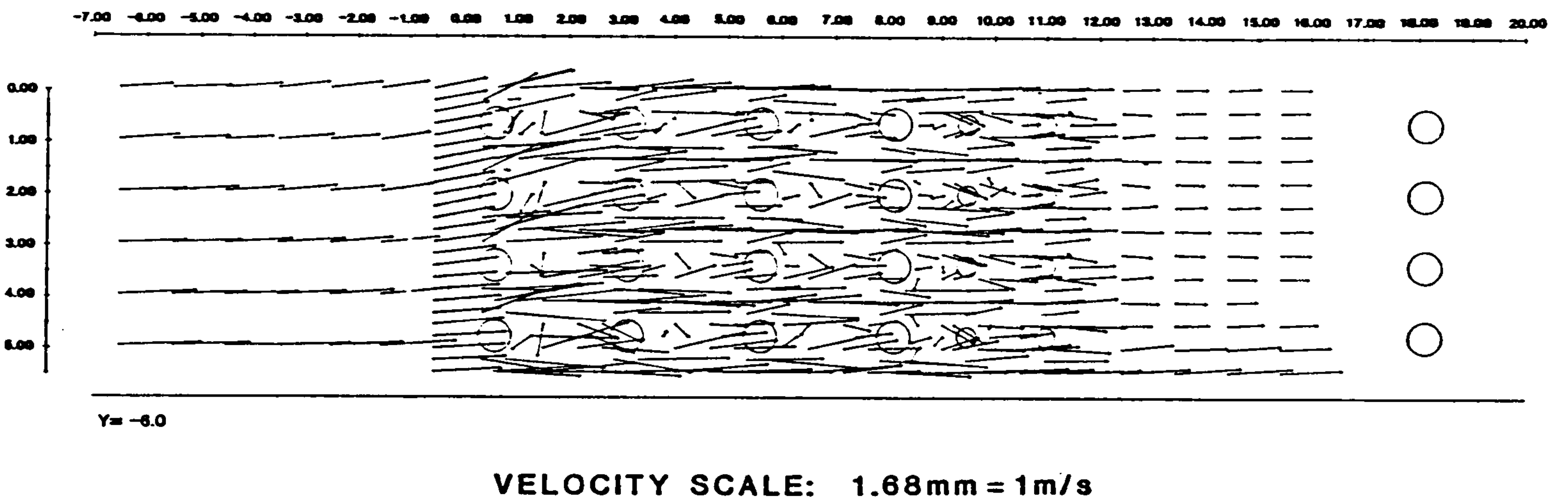

Figure 12. Velocity Field in the Inlet Transition, Test Section 1, and the Cooling Section Entrance at Y = 6.0 inches. (near the bottom of SHTM).

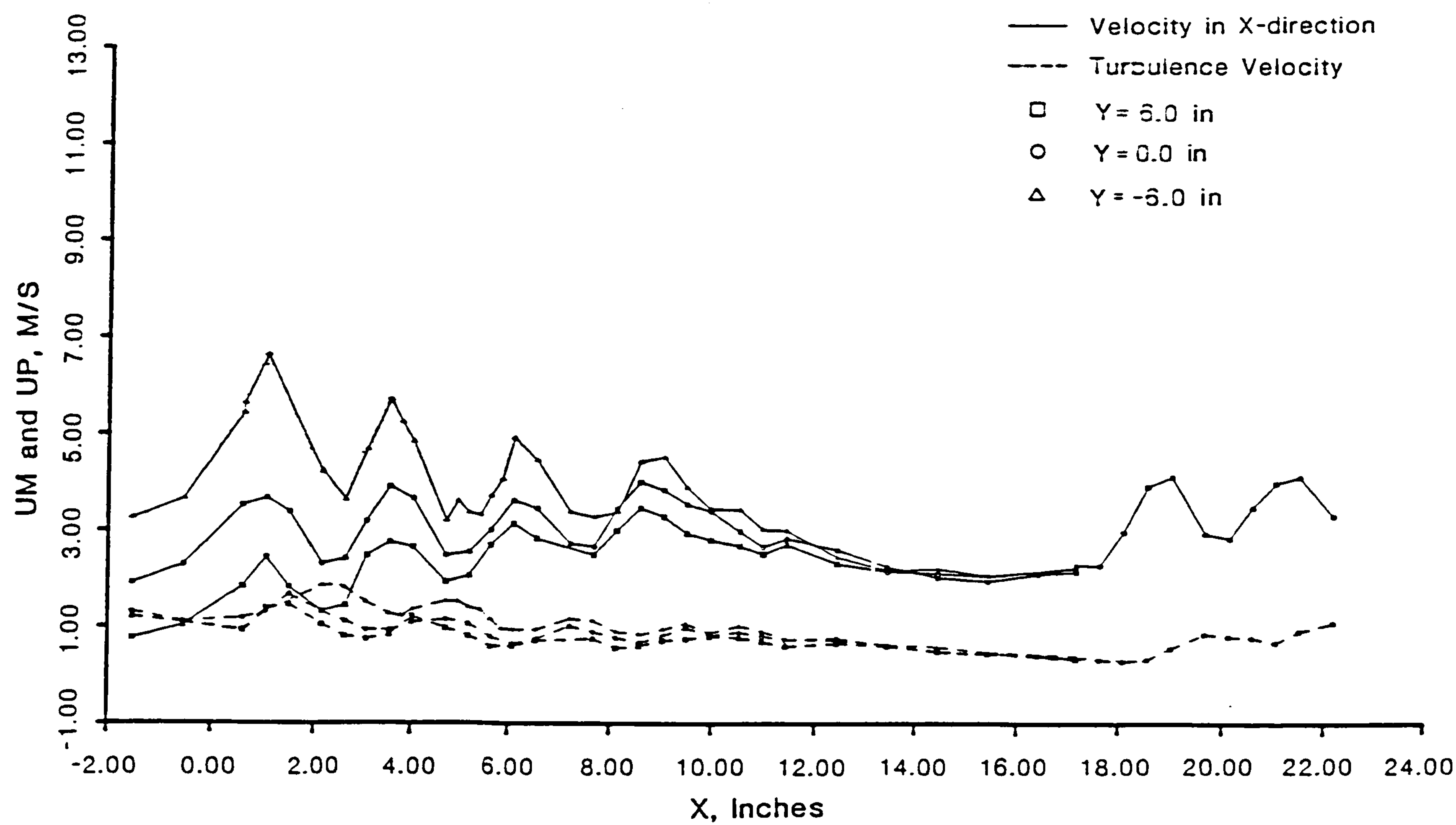

Figure 13. Plot of Mean Velocities and Turbulence Velocities versus Distance at Z = 0.0 inches (in plane of symmetry of SHTM).

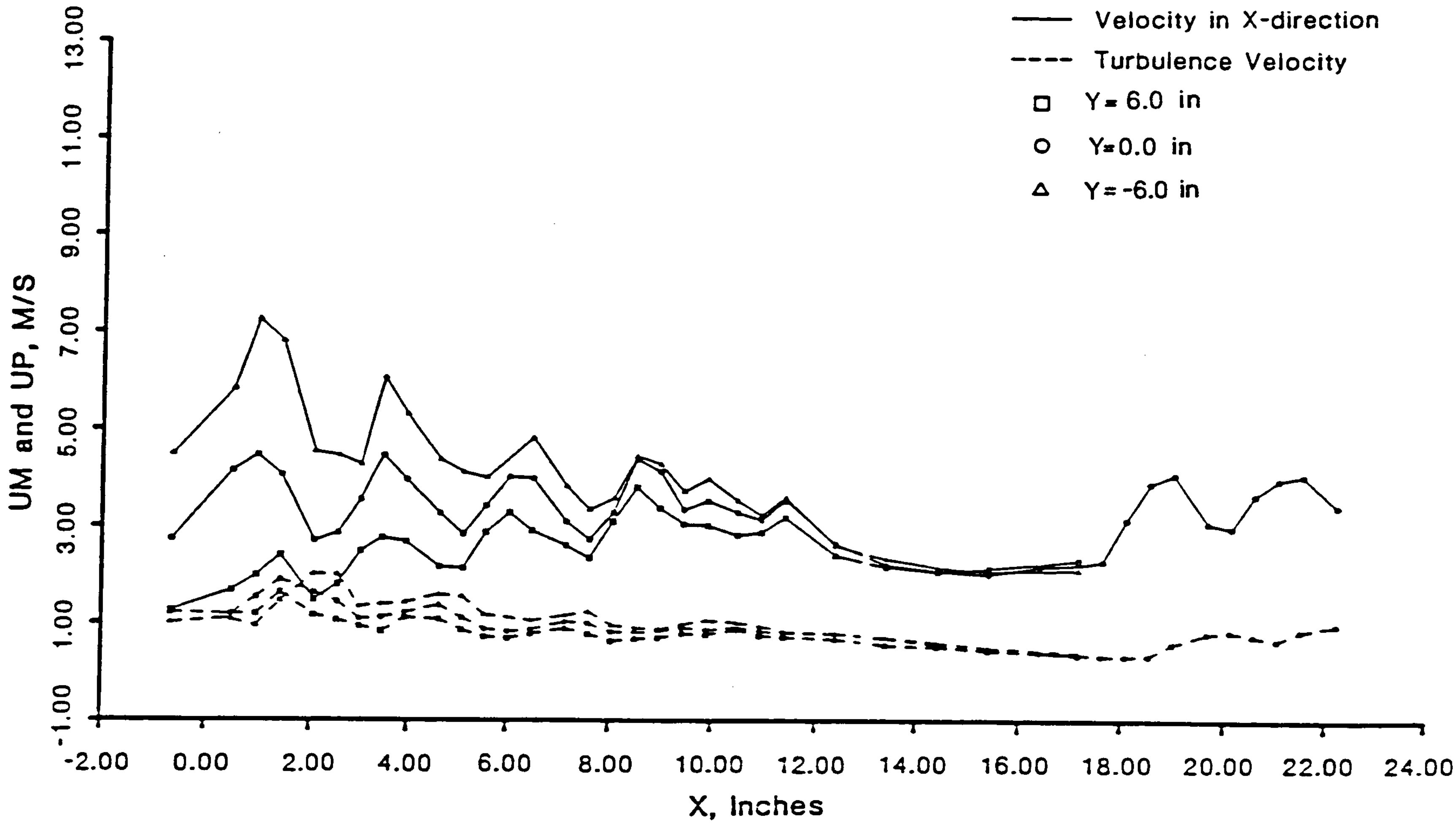

Figure 14. Plot of Mean Velocities and Turbulence Velocities versus Distance at Z = -1.375 inches.

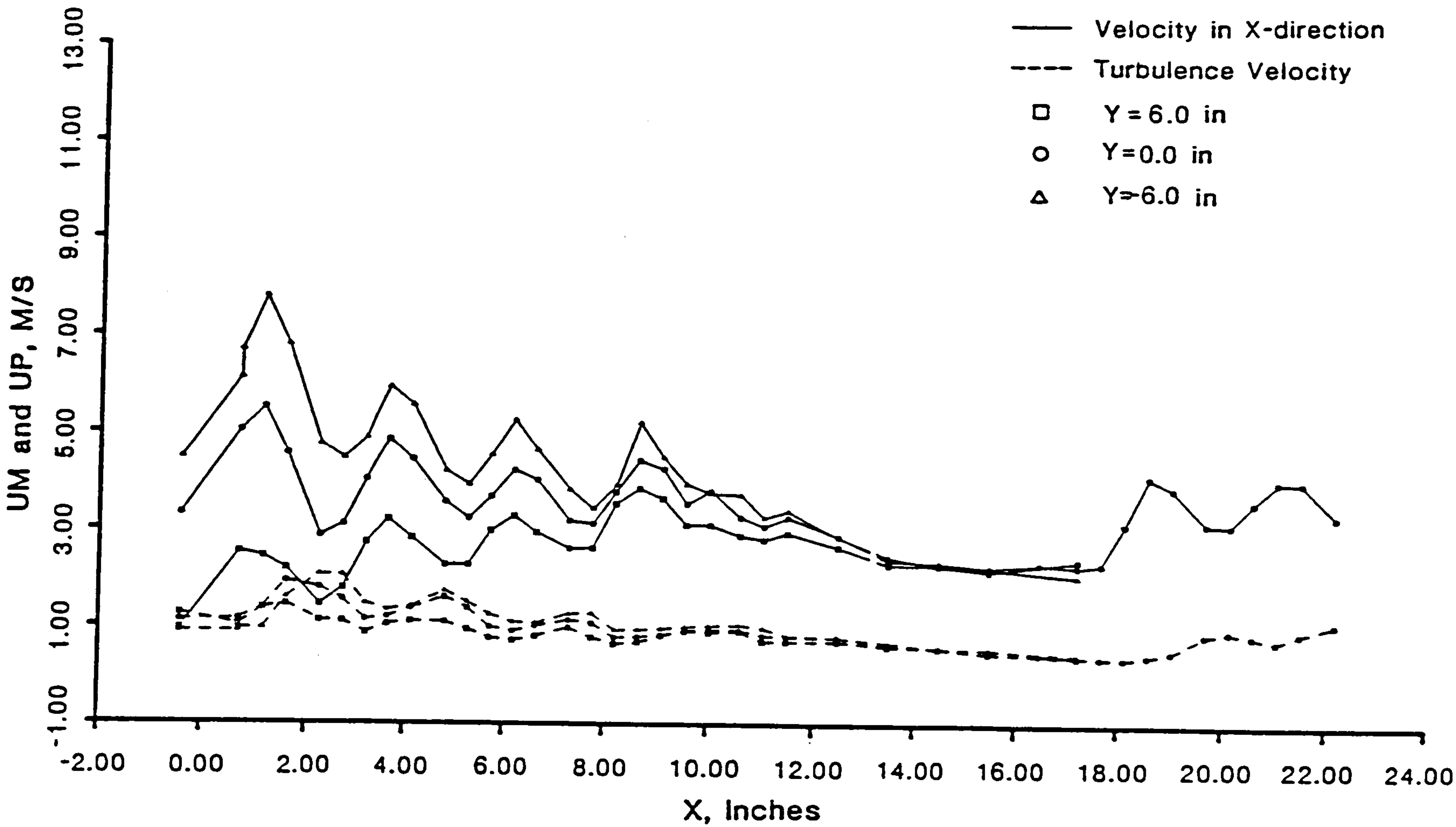

Figure 15. Plot of Mean Velocities and Turbulence Velocities versus Distance at Z = -2.750 inches.

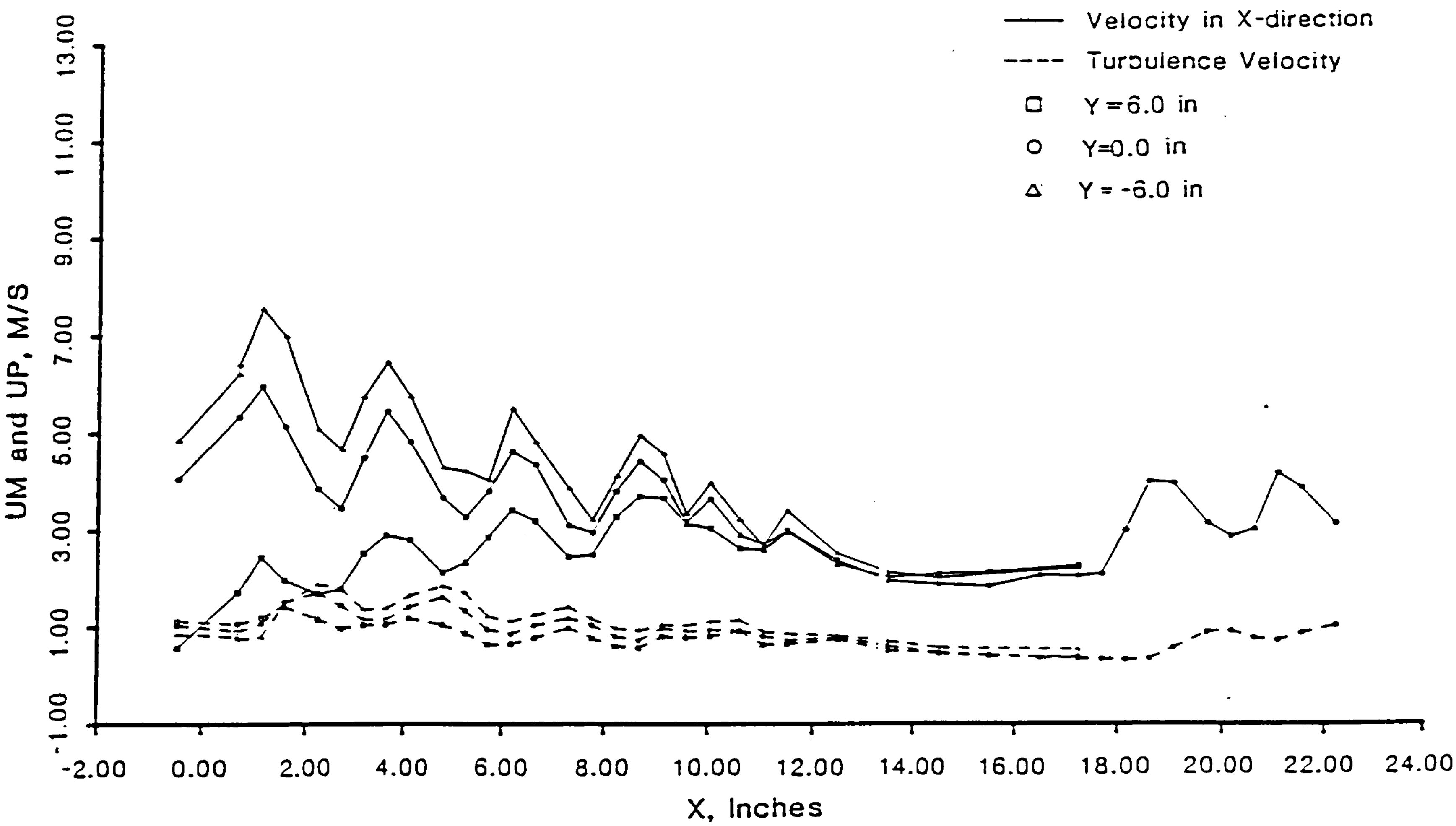

Figure 16. Plot of Mean Velocities and Turbulence Velocities versus Distance at Z = -4.125 inches.

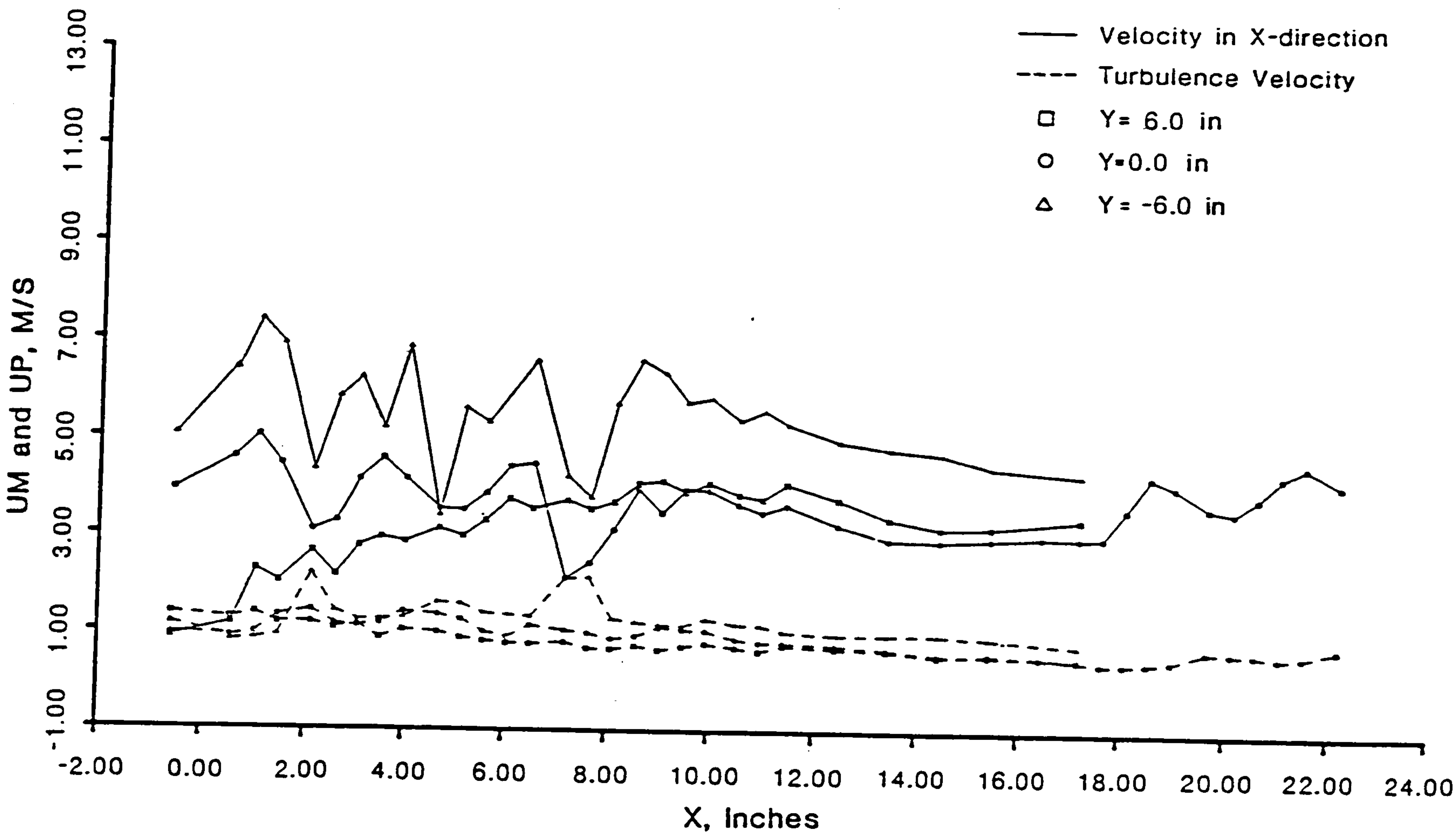

Figure 17. Plot of Mean Velocities and Turbulence Velocities versus Distance at Z = −5.500 inches.

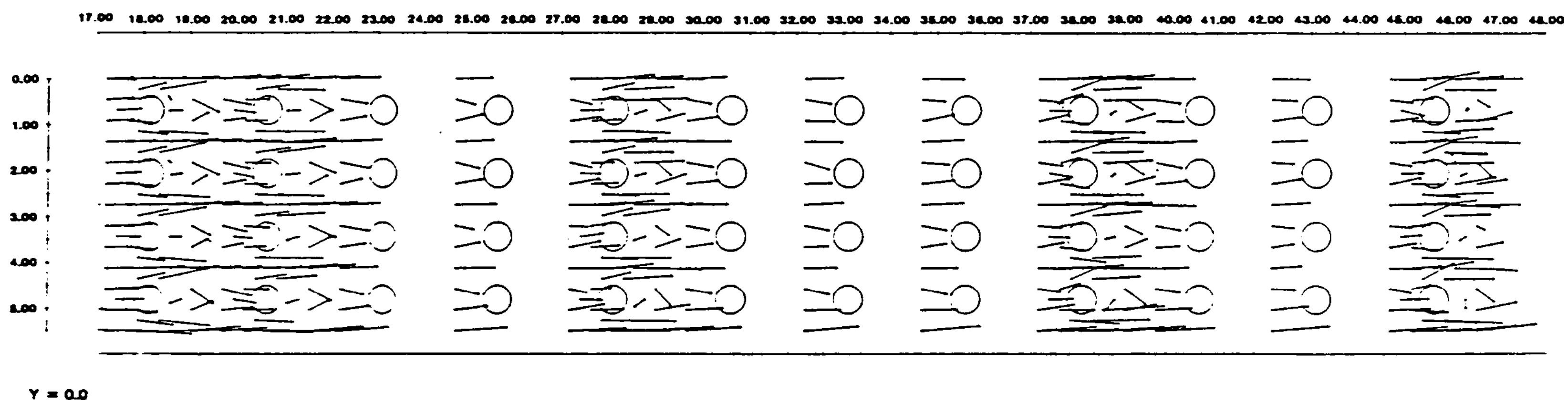

VELOCITY SCALE: 1.68mm = 1m/s

Figure 18. Velocity Field in the Cooling Section at Y = 0.0 inches.

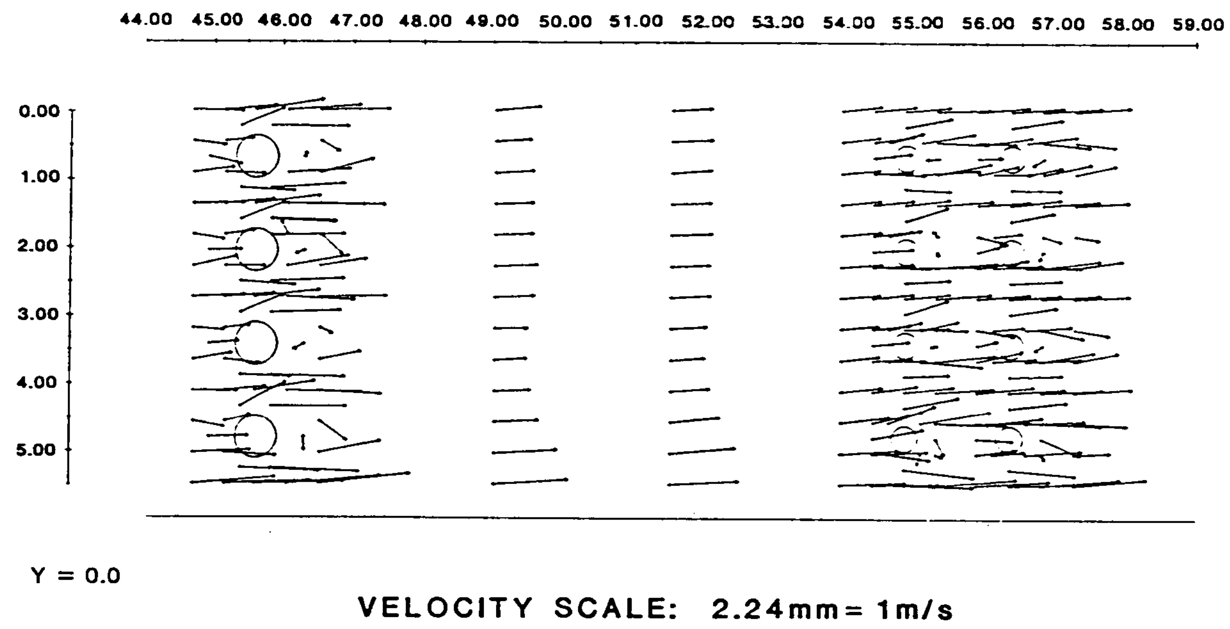

Figure 19. Velocity Field in the Cooling Section Exit and Test Section 2 at Y = 0.0 inches.

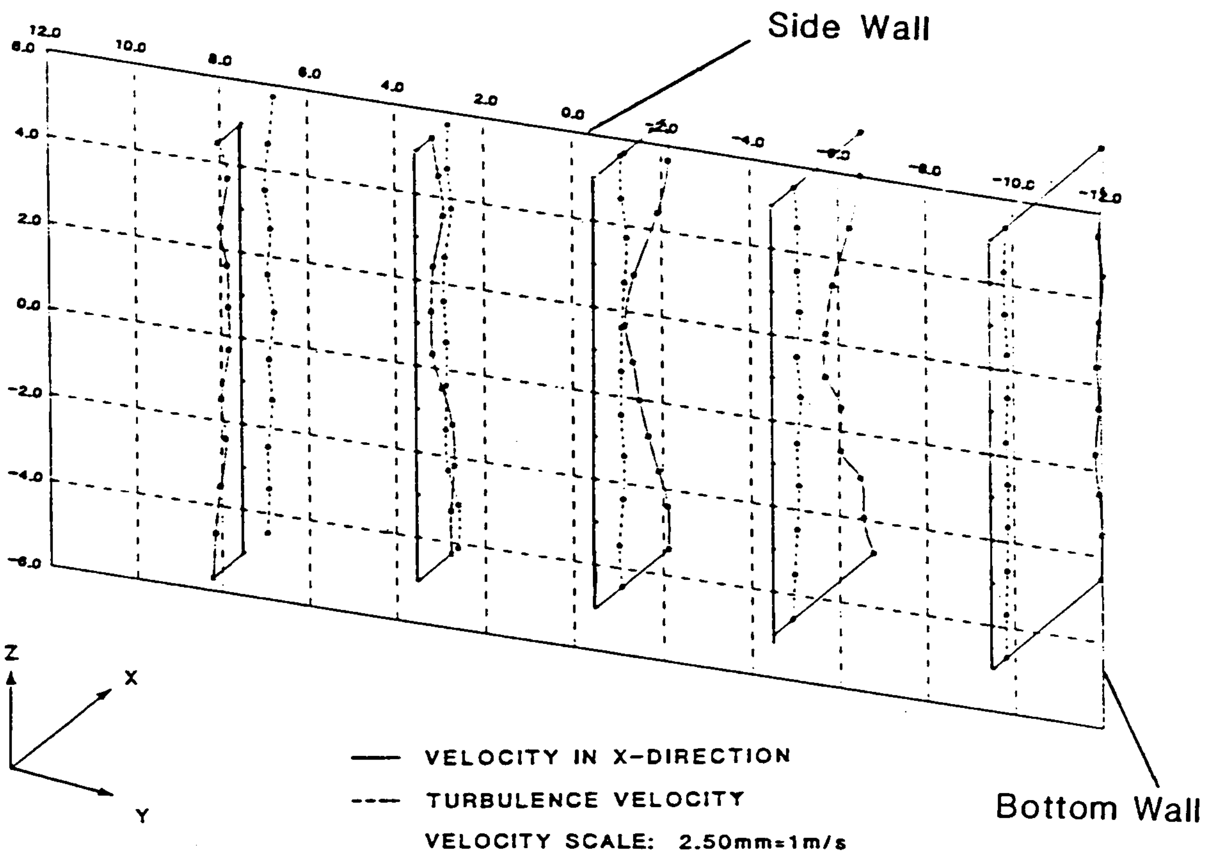

Figure 20. Mean Velocity and Turbulence Velocity Profiles in Cross-sectional Plane at X = -7.5 inches (inlet transition).

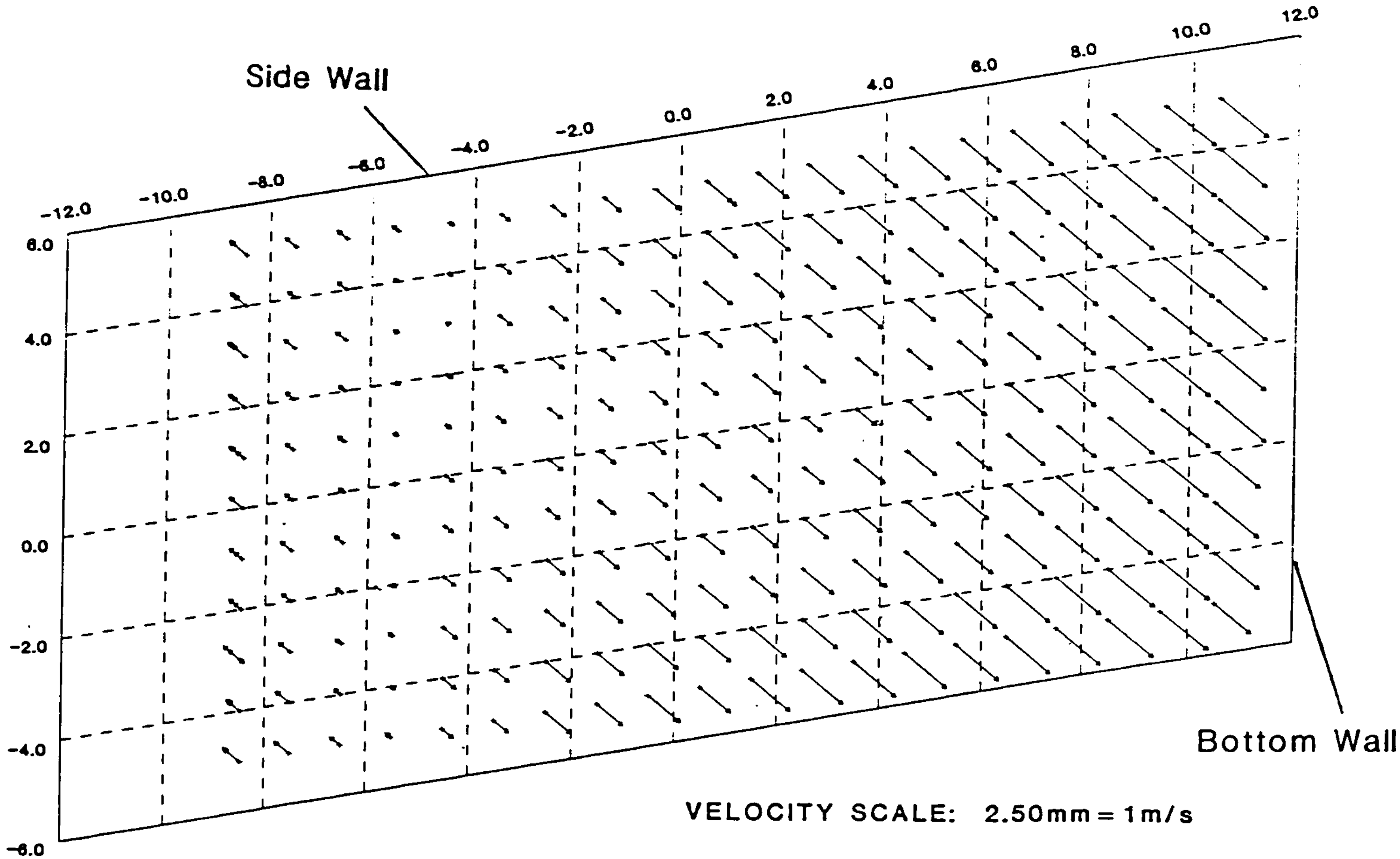

Figure 21. Cross-sectional Vector Velocity Field in Inlet Transition at X = -7.5 inches.

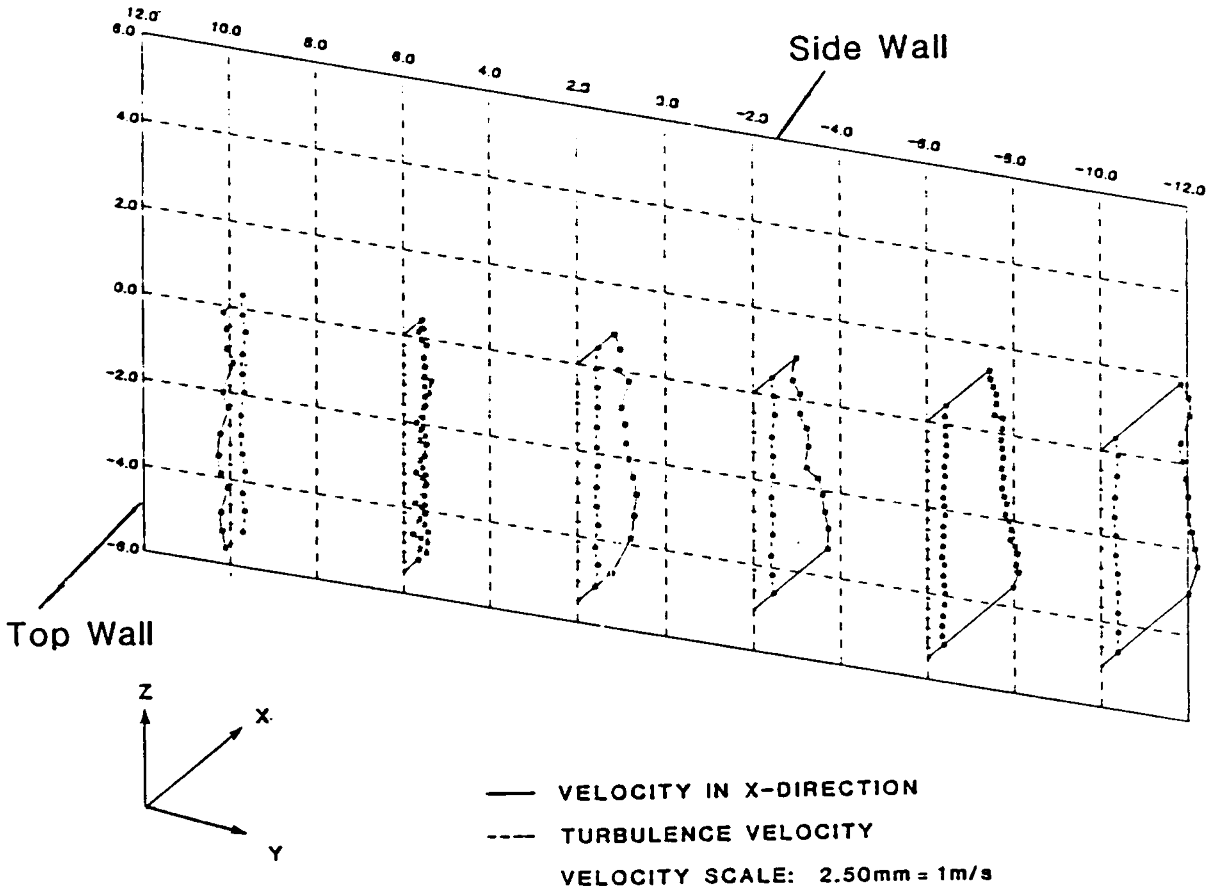

Figure 22. Profiles of Mean Velocity and Turbulence Velocity in Cross-sectional Plane in Front of Cooling Tubes in Test Section 1 at X = -0.521 inches.

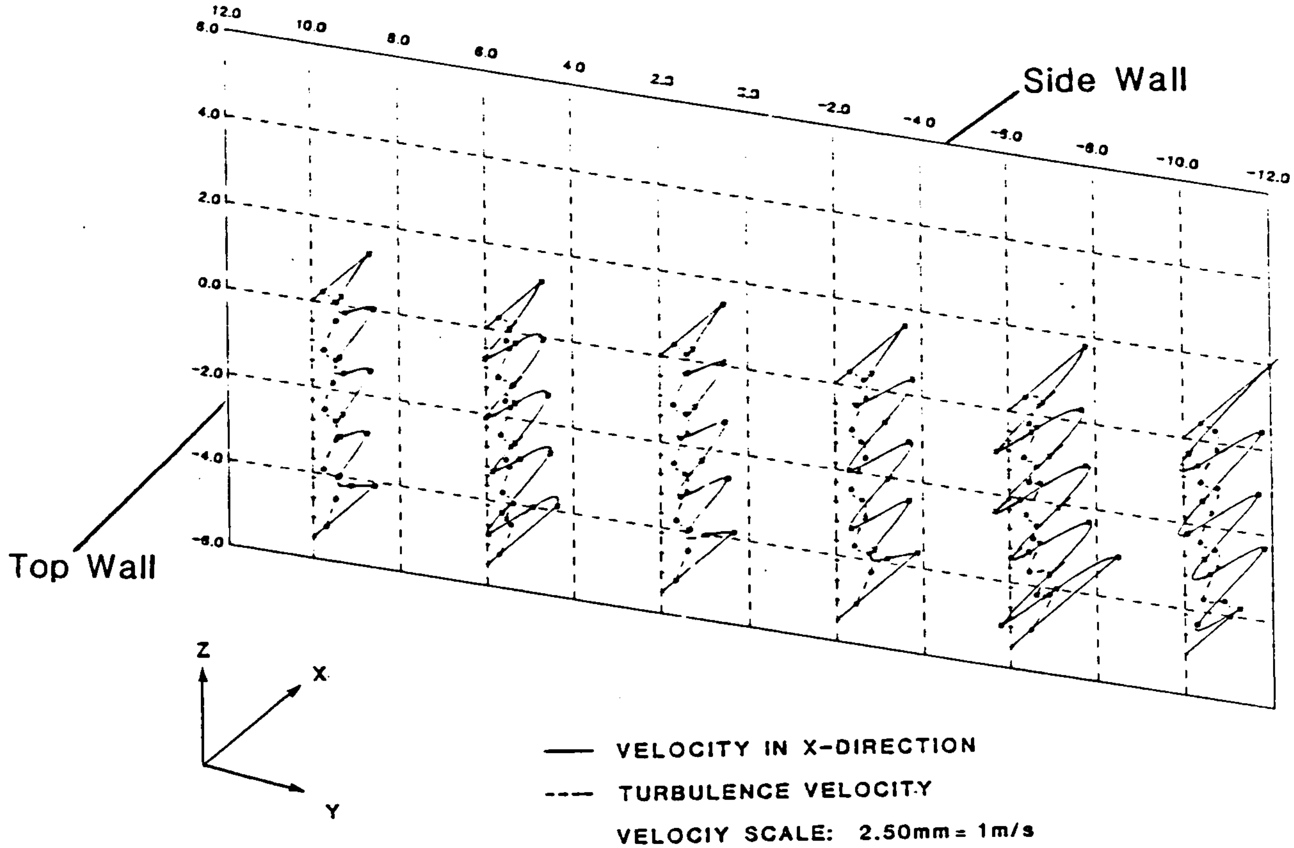

Figure 23. Profiles of Mean Velocity and Turbulence Velocity in Cross-sectional Plane in Test Section 1 Between Cooling Tubes and Steam Tubes at X = 9.042 inches.

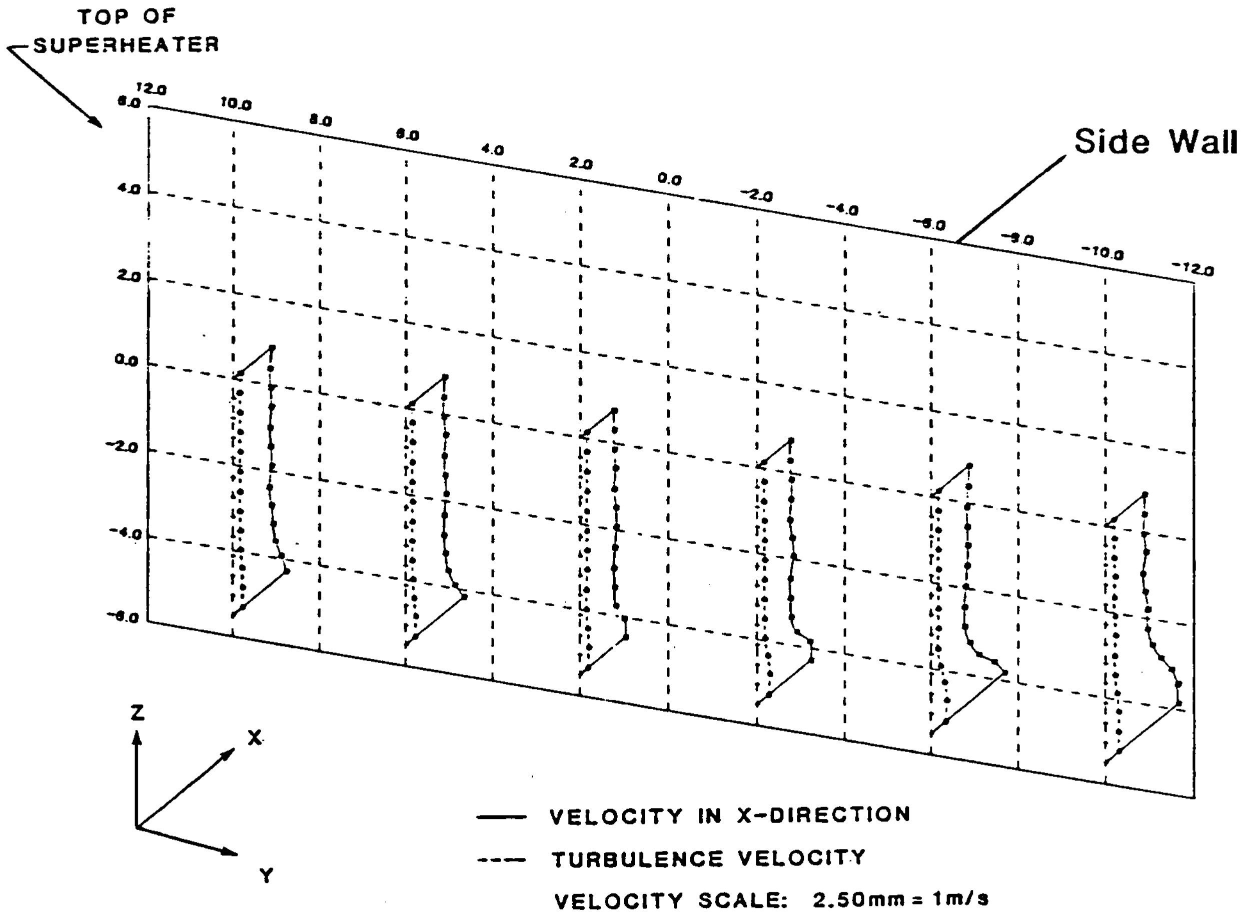

Figure 24. Profiles of Mean Velocity and Turbulence Velocity in Cross-sectional Plane at Cooling Section Entrance at X = 17.208 inches.

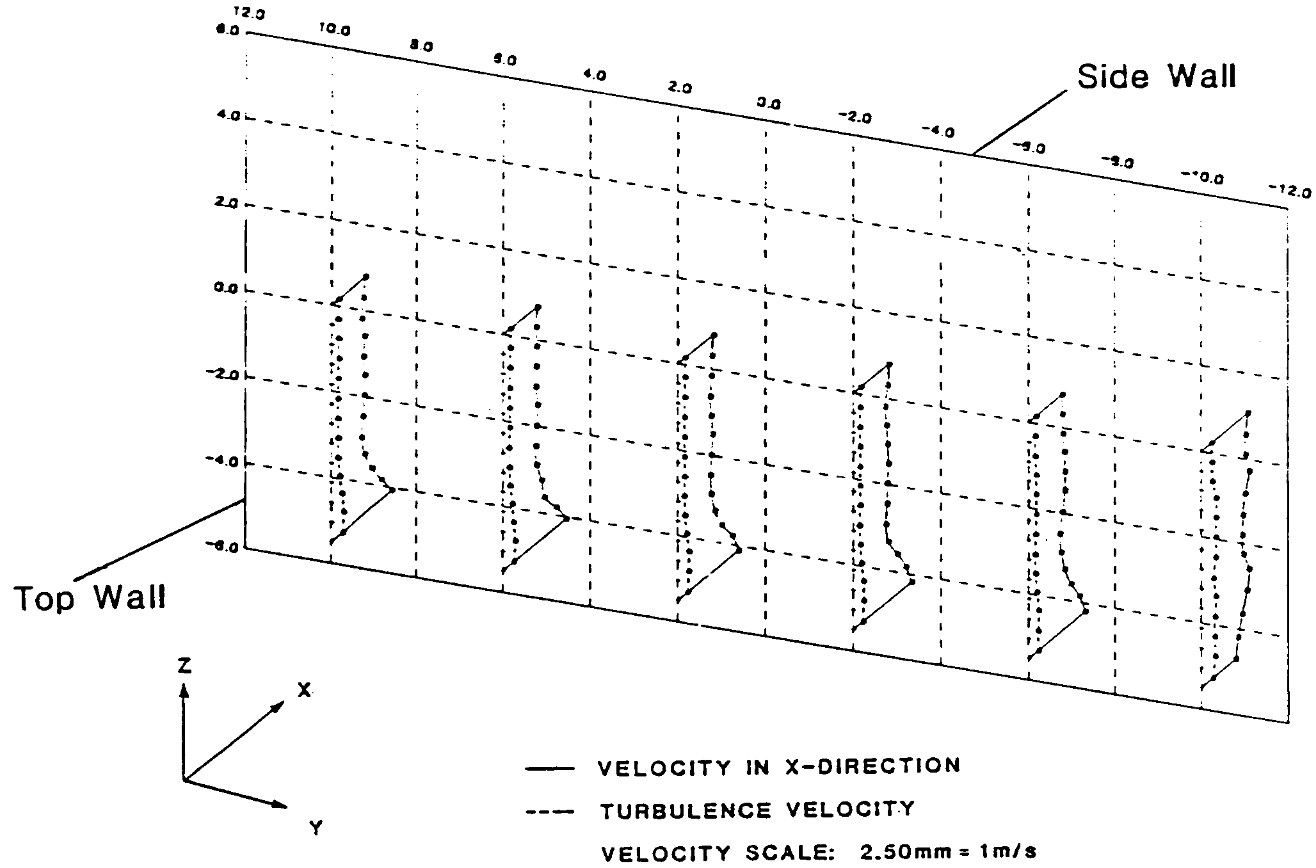

Figure 25. Profiles of Mean Velocity and Turbulence Velocity in Cross-sectional Plane of Test Section 2 in Front of Steam Tubes at X = 53.957 inches.

VITA

Rodney William Hoefer was born in Poplar Bluff, Missouri on March 1, 1961. His family later moved to Union City, Tennessee where he graduated from high school in May, 1979. He received a B.S. degree in Mechanical Engineering Technology from The University of Tennessee at Martin in August, 1983. Since then he has been employed by the Energy Conversion Research and Development Programs at The University of Tennessee Space Institute, Tullahoma, Tennessee where he is working toward his M.S. degree in Mechanical Engineering.

Mr. Hoefer is married to the former Dianna Lynn Farrar of Tullahoma, Tennessee.